

# Development of a Novel, Small-Molecule Brain-Penetrant Histone Deacetylase Inhibitor That Enhances Spatial Memory Formation in Mice

Jawad B. Belayet,<sup>†</sup> Sarah Beamish,<sup>†</sup> Mizzanoor Rahaman,<sup>†</sup> Samer Alanani,<sup>†</sup> Rajdeep S. Viridi, David N. Frick, A. F. M. Towheedur Rahman, Joseph S. Ulicki, Sreya Biswas, Leggy A. Arnold, M. S. Rashid Roni, Eric Y. Cheng, Douglas A. Steeber,\* Karyn M. Frick,\* and M. Mahmun Hossain\*



Cite This: *J. Med. Chem.* 2022, 65, 3388–3403



Read Online

ACCESS |



Metrics & More

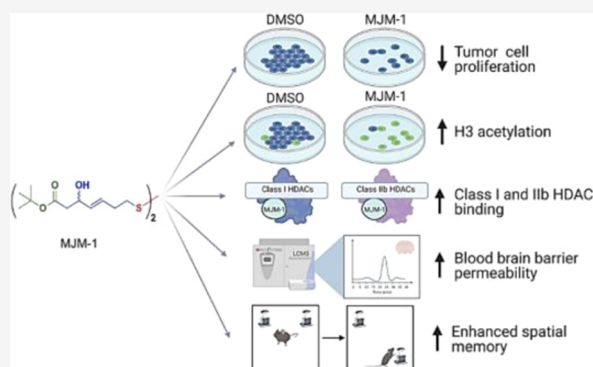


Article Recommendations



Supporting Information

**ABSTRACT:** Histone acetylation is a prominent epigenetic modification linked to the memory loss symptoms associated with neurodegenerative disease. The use of existing histone deacetylase inhibitor (HDACi) drugs for treatment is precluded by their weak blood–brain barrier (BBB) permeability and undesirable toxicity. Here, we address these shortcomings by developing a new class of disulfide-based compounds, inspired by the scaffold of the FDA-approved HDACi romidepsin (FK288). Our findings indicate that our novel compound MJM-1 increases the overall level of histone 3 (H3) acetylation in a prostate cancer cell line. In mice, MJM-1 injected intraperitoneally (i.p.) crossed the BBB and could be detected in the hippocampus, a brain region that mediates memory. Consistent with this finding, we found that the post-training i.p. administration of MJM-1 enhanced hippocampus-dependent spatial memory consolidation in male mice. Therefore, MJM-1 represents a potential lead for further optimization as a therapeutic strategy for ameliorating cognitive deficits in aging and neurodegenerative diseases.



## INTRODUCTION

Memory dysfunction is a common symptom of aging and neuropsychiatric and neurodegenerative disorders, yet truly effective treatments for memory loss do not exist. Memory dysfunction stems, in part, from reduced gene expression that leads to decreased levels of proteins essential for neural plasticity.<sup>1</sup> Within chromatin, DNA is tightly wound around an octamer of four different histone proteins. Acetylation of these proteins relaxes the bond between histones and DNA and leads to chromatin remodeling, thereby increasing gene transcription.<sup>2,3</sup> Histone acetylation in the brain increases the expression of memory-related genes and is required for long-term memory formation.<sup>4,5</sup> Compounds that maintain histone acetylation, called histone deacetylase inhibitors (HDACis), prevent the deacetylation of core histone proteins, thereby promoting a transcriptionally favorable state for the expression of genes that regulate neural plasticity and memory. Therefore, HDACis are promising therapeutics that could be used to prevent or delay memory loss associated with aging and other disorders.<sup>6,7</sup>

Class I HDACs (HDACs 1–3, 8) are extensively expressed in the rat hippocampus and amygdala, both of which are brain regions critical for learning and memory.<sup>8</sup> As such, class I HDACs have been the most studied in the context of

cognition.<sup>9,10</sup> For instance, systemic intraperitoneal (i.p.) injection of the brain-penetrant HDACi sodium butyrate (NaBu) facilitates the formation of long-term object recognition (OR) memory in male mice.<sup>11,12</sup> Similarly, the infusion of the HDACi trichostatin A (TSA) into the dorsal hippocampus enhances object recognition memory in ovariectomized female mice<sup>13</sup> and spatial memory in male mice.<sup>14</sup> These and other HDACis also promote morphological and physiological alterations that lead to increased neural plasticity in the hippocampus and amygdala.<sup>15,16</sup>

Although brain-penetrant HDACi such as NaBu and TSA can improve various forms of memory in rodents, their therapeutic utility in humans remains limited because they lack selectivity toward specific isoforms of HDAC enzymes. This represents a significant challenge in treating neurological disorders, as pan-selective HDACis produce negative side effects and unwanted cytotoxicity because they also target

Received: November 10, 2021

Published: February 8, 2022



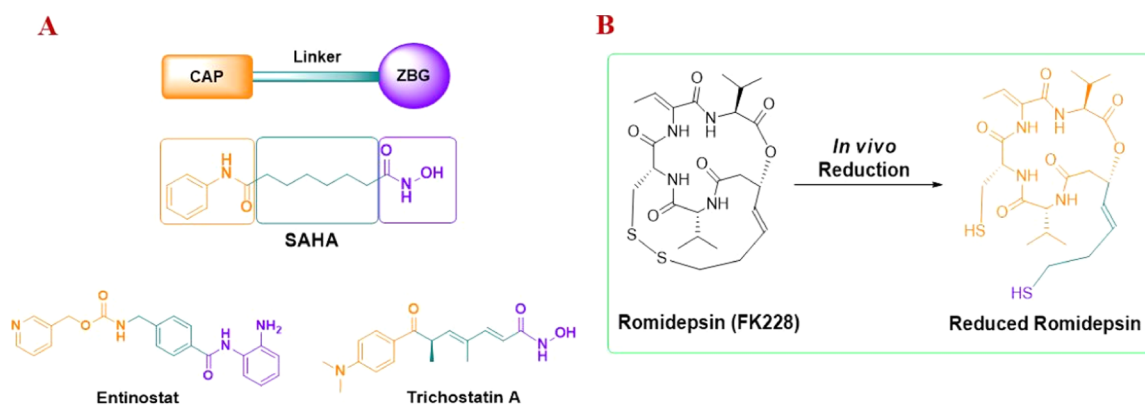
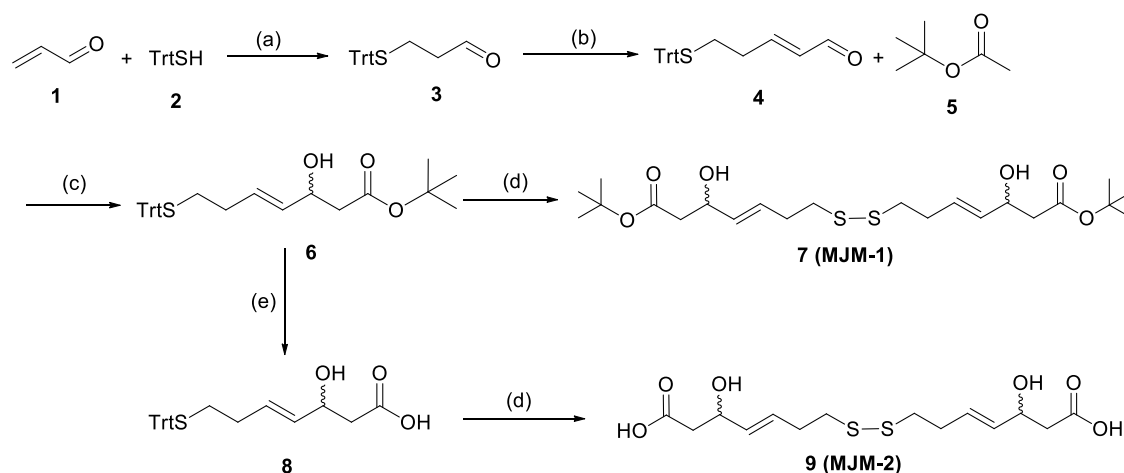


**Figure 1.** Structural analysis of HDAC inhibitors. (A) Pharmacophore model and chemical structures of selected HDAC inhibitors; and (B) romidepsin structure and its reduced active form.

### Scheme 1. Synthesis of MJM-1 and MJM-2<sup>4</sup>



<sup>4</sup>Reagents and conditions: (a) Et<sub>3</sub>N, CH<sub>2</sub>Cl<sub>2</sub>, rt, 3 h; (b) (triphenylphosphoranylidene)acetaldehyde, C<sub>6</sub>H<sub>6</sub>, reflux, 12 h; (c) LDA, THF, −78 °C, 3 h; (d) I<sub>2</sub>, NaOAc, CH<sub>2</sub>Cl<sub>2</sub> : MeOH (10:1), 0 °C to rt, 3 h; (e) LiOH, THF/ H<sub>2</sub>O (4:1), 50 °C, 12 h.

nonhistone proteins such as transcription factors, nuclear transport proteins, and cytoskeleton proteins that can alter cell-cycle progression, differentiation, and apoptosis.<sup>17</sup> Moreover, FDA-approved HDACis that have traditionally been used for the treatment of hematological diseases have limited ability to cross the blood–brain barrier (BBB).<sup>18</sup> Considering these obstacles, the goal of this project was to synthesize small HDACi molecules that easily penetrate the BBB and enhance memory with minimum cytotoxicity.

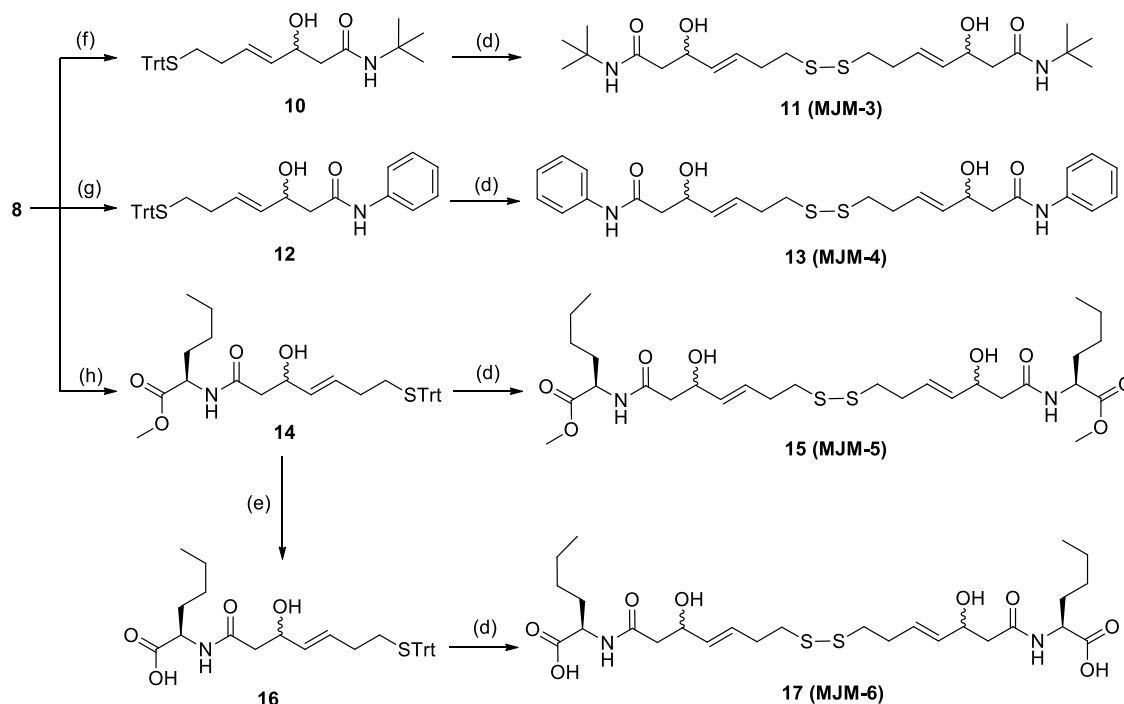
Most HDACis typically follow a common pharmacophore structure that is comprised of a cap group, a linker, and a zinc-binding group (ZBG) (Figure 1A). The crystal structures of HDACi-Zn<sup>2+</sup> complexes illustrated that the zinc-binding groups chelate with a zinc ion (Zn<sup>2+</sup>) located in the catalytic center of HDAC enzymes.<sup>19,20</sup> The linker travels through the narrow hydrophobic channel (11 Å), which connects the ZBG with the surface recognition cap group.<sup>19,21</sup> Modifying these pharmacophore pieces is critical for improving the potency and isoform selectivity of novel HDACi compounds.<sup>22,23</sup> To date, four HDACi compounds (SAHA, romidepsin, belinostat, and panobinostat) have been approved by the FDA as chemotherapeutic agents.<sup>24,25</sup> Although HDACis have been traditionally developed to treat cancer, there are promising applications for the utility of HDACi-based therapeutics to

improve memory deficits associated with neurodegenerative disorders.<sup>26,27</sup>

Based on the typical pharmacophore model, we demonstrate in this series of studies the development and biological evaluation of a new class of disulfide-based HDACis. Initial biological assessment of the target compounds included assays of cell viability, histone 3 (H3) acetylation, HDAC inhibition by the lead compound, MJM-1, *in vitro*, and in a cancer cell line. The lead compound was then subjected to *in vivo* studies to evaluate its BBB penetration capability. Upon finding that MJM-1 penetrates the BBB and is detected in the hippocampus, the ability of MJM-1 to enhance memory formation was assessed in tasks that rely on hippocampal function.

## RESULTS

**Chemistry: Structural Design and Synthesis.** To date, a range of natural and synthetic HDACis have been identified, which are structurally diverse. Among them, cyclic depsipeptide-type HDACis are complex natural products containing a large macrocyclic framework.<sup>28</sup> The depsipeptide (e.g., romidepsin)-type inhibitors are structurally unique, as they serve as stable prodrugs, and upon intracellular reduction of the disulfide bond by glutathione, they convert to its active monocyclic dithiol form (Figure 1B). The freed thiol group

Scheme 2. Synthesis of MJM-3, MJM-4, MJM-5, and MJM-6<sup>a</sup>

<sup>a</sup>Reagents and conditions: (d) I<sub>2</sub>, NaOAc, CH<sub>2</sub>Cl<sub>2</sub> : MeOH (10:1), 0 °C to rt, 3 h; (e) LiOH, THF/ H<sub>2</sub>O (4:1), 50 °C, 12 h; (f) *tert*-butyl amine, PyBOP, DIPEA, CH<sub>2</sub>Cl<sub>2</sub>, 0 °C to rt, 12 h; (g) EDC, DMAP, TEA, phenyl amine, CH<sub>2</sub>Cl<sub>2</sub>, 0 °C to rt, 12 h; (h) *D*-norleucine methyl ester hydrochloride, PyBOP, DIPEA, CH<sub>2</sub>Cl<sub>2</sub>, 0 °C to rt, 12 h.

with the longer aliphatic linker enters the catalytic pocket and chelates with zinc, thus inhibiting the enzyme activities.<sup>29</sup>

Although romidepsin was found to be highly potent against certain malignancies, it shows high cytotoxicity and very low BBB permeability, highlighting its drawbacks in clinical applications for neurodegenerative diseases.<sup>30</sup> To improve BBB permeability of HDAC inhibitors, most efforts have been focused on increasing lipophilicity.<sup>31,32</sup> In this endeavor, we hypothesized that certain designer small compounds inspired by the romidepsin scaffold may possess more “druglike” properties, such as increased solubility/bioavailability, decreased toxicity, and high brain uptake upon i.p. administration, yet be adequately potent to benefit memory formation. Therefore, we set out to design small HDACis that are structurally derived from romidepsin by following the typical pharmacophore model. Accordingly, we made HDACi bearing the C6 linker with a smaller cap group while still containing a disulfide bond as in romidepsin, which should act by the same prodrug mechanism.<sup>33</sup>

Our synthesis started with the commercially available acrolein for the formation of the desired disulfide compounds **7** (MJM-1) and **9** (MJM-2) following the synthetic route shown in Scheme 1. Initially, the reaction between acrolein **1** and triphenylmethanethiol **2** afforded aldehyde **3**. The corresponding α,β-unsaturated aldehyde **4** was then prepared by the Wittig reaction between **3** and 2-(triphenylphosphoranylidene)acetaldehyde. The desired aldol product **6** was achieved from **4** using lithium diisopropylamide (LDA) [generated in situ by reaction with *n*-BuLi and diisopropyl amine (DIPEA)] as a base and *tert*-butyl ester **5** as the enolate source. The aldol reaction provided the β-hydroxy ester **6** as a racemic mixture. Subsequently, the racemic product **6** then underwent a dimerization reaction in

the presence of iodine and sodium acetate, resulting in the desired disulfide product MJM-1. The racemic ester **6** was then deprotected with lithium hydroxide to yield β-hydroxy acid **8**, from which the expected disulfide product MJM-2 was obtained by applying the same dimerization reaction conditions as described earlier.

In the next phase, we aimed to modify the cap group by replacing the ester moiety with an amide functionality through a coupling reaction (Scheme 2). First, β-hydroxy acid **8** and phenylamine were placed under coupling conditions using benzotriazol-1-yl-oxytripyrrolidinophosphonium hexafluorophosphate (PyBOP) as a coupling reagent and *N,N*-diisopropyl ethyl amine (DIPEA) as a base, which led to the formation of corresponding amides **12**. Unfortunately, the same coupling condition did not work well for a *tert*-butyl amide. To synthesize compound **10**, different coupling conditions were applied during the reaction between *tert*-butylamine and **8**, where 1-(3-dimethylaminopropyl)-3-ethylcarbodiimide hydrochloride (EDC) was used as a coupling reagent, triethylamine (TEA) as a base, and 4-dimethylaminopyridine (DMAP) as a catalyst. Later, we incorporated a bigger cap group by the coupling of β-hydroxy acid **8** and *D*-norleucine methyl ester hydrochloride by employing the same coupling conditions used for compound **10**, which yielded compound **14**. The basic hydrolysis of ester **14** resulted in the corresponding acid **16**. Finally, applying the similar dimerization condition mentioned in Scheme 1, the desired dimer compounds MJM-3, MJM-4, MJM-5, and MJM-6 were synthesized from **10**, **12**, **14**, and **16**, respectively.

**Biological Evaluation.** The ability of each “MJM” compound to inhibit deacetylation reactions catalyzed by HDAC2 *in vitro* was monitored in a concentration-dependent manner in the presence and absence of the reducing agent

dithiothreitol (DTT). DTT was assumed to reduce each compound to its active (SH) monomer form, as depicted for romidepsin (Figure 1B). The addition of DTT increased the potency of each compound, typically about 10-fold (Table 1). DTT did not affect HDAC activity when added to dimethyl sulfoxide (DMSO) alone.

**Table 1. HDAC2 Inhibition of MJM Compounds Synthesized in the Presence and Absence of the Reducing Agent DTT**

compound	IC <sub>50</sub> (μM) <sup>a</sup>	
	+DTT	-DTT
MJM-1	10 ± 4	100 ± 20
MJM-2	28 ± 19	140 ± 40
MJM-3	18 ± 11	>100
MJM-4	25 ± 8	105 ± 60
MJM-5	17 ± 6	280 ± 130
MJM-6	11 ± 6	140 ± 30

<sup>a</sup>Concentration needed to inhibit HDAC2 by 50% in an HDAC-Glo assay. Values determined from two independent titrations with each HDACi (average ± standard deviation, SD). >100, less than 50% inhibition at the highest concentration tested.

To study the effects of MJM compounds after 48 h in respect to cell proliferation, a 3-(4,5-dimethylthiazol-2-yl)-2,5-diphenyltetrazolium bromide (MTT) assay was conducted on DU145 tumor cell (Figure 2). Romidepsin was used as a

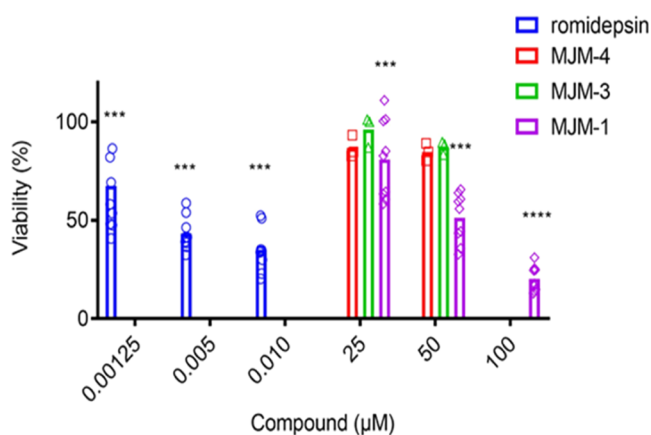


**Figure 2.** DU145 tumor cells showed decreased viability after treatment with MJM-1. DU145 tumor cells were treated with the indicated concentration of MJM-4 (squares), MJM-3 (triangles), MJM-1 (diamonds), or romidepsin (circles) for 48 h. Absorbance values were obtained and normalized to DMSO control levels. Percent of cells remaining was calculated, and results are representative of three independent experiments. Only MJM-1 showed significantly reduced cell viability (\*\*\**p* < 0.0001) at 100 and at 50 μM (\*\*\**p* = 0.0006) compared to DMSO. Romidepsin was used as a positive control and demonstrated significantly reduced viability (\*\*\**p* = 0.0002) at 10 and 5 nM. Bars indicate the mean percent inhibition.

positive HDACi control. Interestingly, only MJM-1 showed concentration-dependent effects on viability (Figure 2). For example, MJM-3 and MJM-4 showed no inhibition of DU145 cell proliferation at the tested concentrations. Other analogues were tested similarly (data not shown) and achieved no significant reduction of cellular proliferation up to 50 μM of

the compound. By contrast, MJM-1 inhibited the growth of DU145 tumor cells in a concentration-dependent manner, with an LD<sub>50</sub> of 39 ± 20 μM. Specifically, the treatment of DU145 tumor cells with 50 μM of MJM-1 significantly reduced proliferation by ~50% and ~80% when treated with 100 μM compared to that of DMSO control. As expected, romidepsin inhibited proliferation in the nM range where concentrations of 5 and 10 nM showed significant inhibition of viability. Based on these results, MJM-1 was selected for further investigation.

Additional cell-based and *in vitro* methods were used to characterize the HDAC inhibitory activity of MJM-1 (Figure 3). First, the acetylation levels of histone H3 were assessed using immunofluorescence microscopy after 24 h of treatment with either DMSO only (Figure 3A), 25 μM (Figure 3B), 50 μM (Figure 3C), or 100 μM MJM-1 (Figure 3D), or 10 nM romidepsin (Figure 3E). Acetylation levels of histone H3 showed a dose-dependent increase following MJM-1 treatment in DU145 tumor cells. Specifically, treatment with 100 and 50 μM of MJM-1 showed many brightly fluorescent nuclei in every field of view, indicating high levels of acetylation. Treatment with 25 μM of MJM-1 resulted in fewer strongly labeled nuclei. As expected, romidepsin treatment also showed increased histone H3 acetylation at the 10 nM dose. Therefore, these results show that the dose-dependent inhibition increased histone H3 acetylation at the 10 nM dose. Therefore, these results show that the dose-dependent inhibition of cell proliferation observed following treatment with MJM-1 correlates with increased levels of histone H3 acetylation. The effect of MJM-1 on the activity of recombinant purified HDACs was also compared with that of romidepsin (Figure 3F). Despite being less potent, MJM-1 inhibited all HDACs including those not in class I. About 100 times more romidepsin, which was developed as a specific class I HDAC inhibitor, was needed to inhibit cytoplasmic class IIb HDAC6 than was needed to inhibit class I HDACs. In contrast, MJM-1 inhibited both class IIb and all class I HDACs tested with similar potency. The lower potency MJM-1 most likely results from the absence of half of the ring present in romidepsin (Figure 1B).

**Maximum Tolerated Dose (MTD) Studies.** To determine the MTD *in vivo*, escalating doses of MJM-1, romidepsin, and SAHA were injected i.p. into BALB/c mice, and morbidity and mortality were monitored over 2 weeks. Romidepsin showed very high toxicity, with the animals only being able to tolerate doses of 3.125 mg/kg (Table 2). By contrast, MJM-1 had an MTD of more than 200 mg/kg, which was similar to that of SAHA, suggesting that both MJM-1 and SAHA are much less toxic than romidepsin.

**MJM-1 Detection in Hippocampus.** Based on the promising anti-HDAC activity in the DU145 prostate cancer cell line and the high maximum tolerable dose, we then decided to examine the extent to which MJM-1 can be detected in blood, liver, and brain samples collected from BALB/c mice. After i.p. injection of 40 mg/kg MJM-1, blood, liver, and brain samples were collected 10, 30, and 60 min following i.p. injection. The samples were analyzed by mass spectroscopy (Shimadzu LCMS-8040), and MJM-1 was detected in all samples. The presence of MJM-1 in brain samples suggests that it can cross the blood–brain barrier (BBB).

Because the hippocampus is responsible for many aspects of memory formation, we further investigated the extent to which a systemic injection of MJM-1 penetrates the hippocampus.

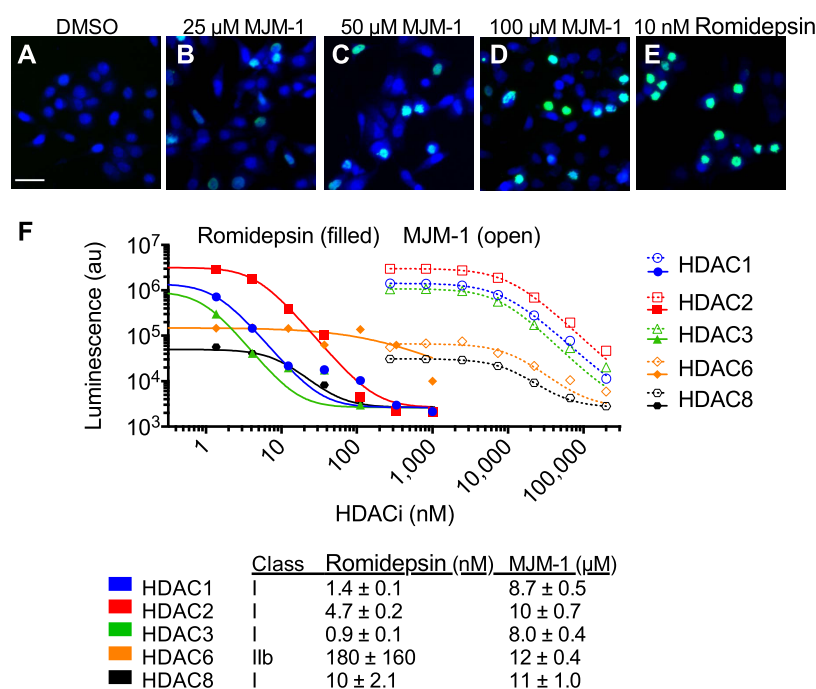


**Figure 3.** Ability of MJM-1 to inhibit HDAC activity. (A–E) Representative images of histone H3 acetylation after treatment with MJM-1 or romidepsin. DU145 tumor cells were treated with the indicated concentrations of MJM-1 or romidepsin for 24 h. Cells were labeled with DAPI (blue) to identify nuclei and stained for acetylated H3 (green). Cells treated with (A) DMSO, (B) 25 μM MJM-1, (C) 50 μM MJM-1, (D) 100 μM MJM-1, and (E) 10 nM romidepsin. Scale bar = 50 μm. (F) Ability of HDAC1 (circles), HDAC2 (squares), HDAC3 (triangles), HDAC6 (diamonds), or HDAC8 (hexagons) to deacetylate peptides in the presence of either romidepsin (filled symbols) or MJM-1 (open symbols). All reactions were performed in triplicate, with averages plotted and fitted to a concentration-response equation using nonlinear regression (GraphPad Prism). The table lists the concentration of either romidepsin or MJM-1 needed to inhibit HDAC-catalyzed reactions by 50% (IC<sub>50</sub>). Deacetylation was coupled to aminoluciferin and luciferase such that luminescence (arbitrary units, au) linearly reflects deacetylase activity. Each reaction contained the same HDAC concentration (0.5 nM) and indicated amounts of a HDACi. Note both axes are log scales. Uncertainties reflect 95% confidence intervals of the curve fits.

**Table 2. Maximum Tolerated Doses**

compound	maximum tolerated dose <sup>a</sup>
SAHA	>200 mg/kg
Romidepsin	3.1 mg/kg
MJM-1	>200 mg/kg

<sup>a</sup>Compounds were dissolved in 20% DMSO/saline and injected i.p. into healthy BALB/c mice. Individual values were derived from the average of triplicate experiments with standard error within a 20% margin. >200, animal survival at the highest concentration tested (200 μM).

MJM-1 was administered i.p. at two different doses (20 or 40 mg/kg) to determine the optimal dose range for subsequent memory assessment. For the 20 mg/kg dose, whole brains were collected from two BALB/c mice for one time point (10 min), whereas for the 40 mg/kg dose, brains were collected at two time points (10 and 30 min). Later, the hippocampus was isolated from each brain. Finally, the hippocampus and the rest of the brain (see the Supporting Information) were analyzed using mass spectroscopy (Shimadzu LCMS-8040) and the chromatograms are shown in Figure 4. For both the 20 mg/kg (see the Supporting Information) and 40 mg/kg dose, MJM-1 was detected 10 min after injection. In addition, for the 40 mg/kg dose, the smaller area of the chromatogram after 30 min suggests a declining amount of MJM-1 in the dorsal hippocampus over time. The data illustrated in Figure 4 suggest that MJM-1 penetrates the BBB and diffuses into the hippocampus rapidly after i.p. administration.

**Pharmacokinetic Study of MJM-1.** After an i.p. injection of 40 mg/kg MJM-1, we detected MJM-1 in blood, brain, and liver with a  $t_{max}$  of ~10 min and  $C_{max}$  values of 131.2, 82.5, and 530 ng/mL, respectively. The calculated half-life in blood, brain, and liver was 45.4, 13.4, and 41 min, respectively. MJM-1 showed the highest area under the curve (AUC) of 31 091 ng/(min mL) for liver, whereas, for brain and blood samples, the AUC was 2019 and 5286 ng/(min mL), respectively. The elimination rate was 0.052 min<sup>-1</sup> in the brain in contrast to that of blood (0.022 min<sup>-1</sup>) and liver (0.017 min<sup>-1</sup>). The plasma:brain ratio was 1:0.38 in terms of AUC (Figure 5A–C).

**Assessment of Memory Consolidation.** We then assessed the extent to which MJM-1 can enhance memory consolidation in male mice. As described in the Experimental Section, the object placement (OP) and object recognition tasks were used to assess spatial and object recognition memory consolidation, respectively.

Briefly, each task consists of a training phase in which mice must accumulate 30 s, exploring two identical objects in an open field (Figure 6A,B). Immediately after training, mice were injected i.p. with vehicle control (DMSO), the positive HDACi control sodium butyrate (NaBu), or one of three doses of MJM-1 (20, 30, 40 mg/kg). Memory in object placement and object recognition was tested 24 and 48 h later, respectively, because negative control mice no longer remember the identity and location of the objects at these time points.<sup>34–36</sup> During object placement testing, one training object was moved to a new location in the testing arena, whereas during object recognition testing, one training object was replaced with a

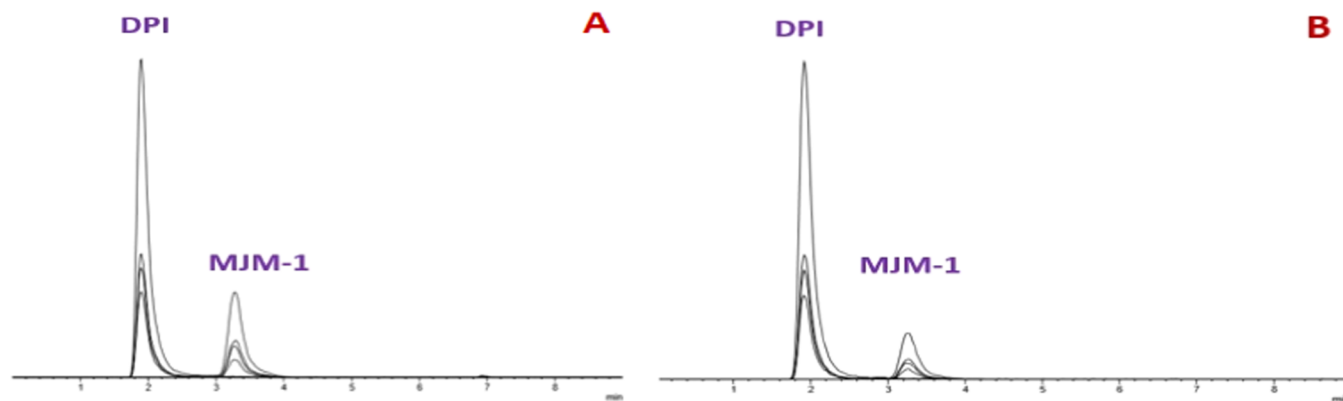


**Figure 4.** Mass chromatogram of MJM-1 (40 mg/kg dose) and internal standard (DPI: 4,5-diphenylimidazole) in hippocampus for two different time points. (A) Sample collected 10 min after i.p. injection. (B) Sample collected 30 min after i.p. injection. The following transitions were monitored in multiple reaction monitoring (MRM) modes for MJM-1:  $m/z$  485  $[M + Na^+] > 373.00$ ,  $m/z$  485  $[M + Na^+] > 429.00$ ,  $m/z$  485  $[M + Na^+] > 311.00$ ; and for DPI:  $m/z$  221  $> 193.00$ ,  $m/z$  221  $> 167.00$ ,  $m/z$  221  $> 152.00$ .

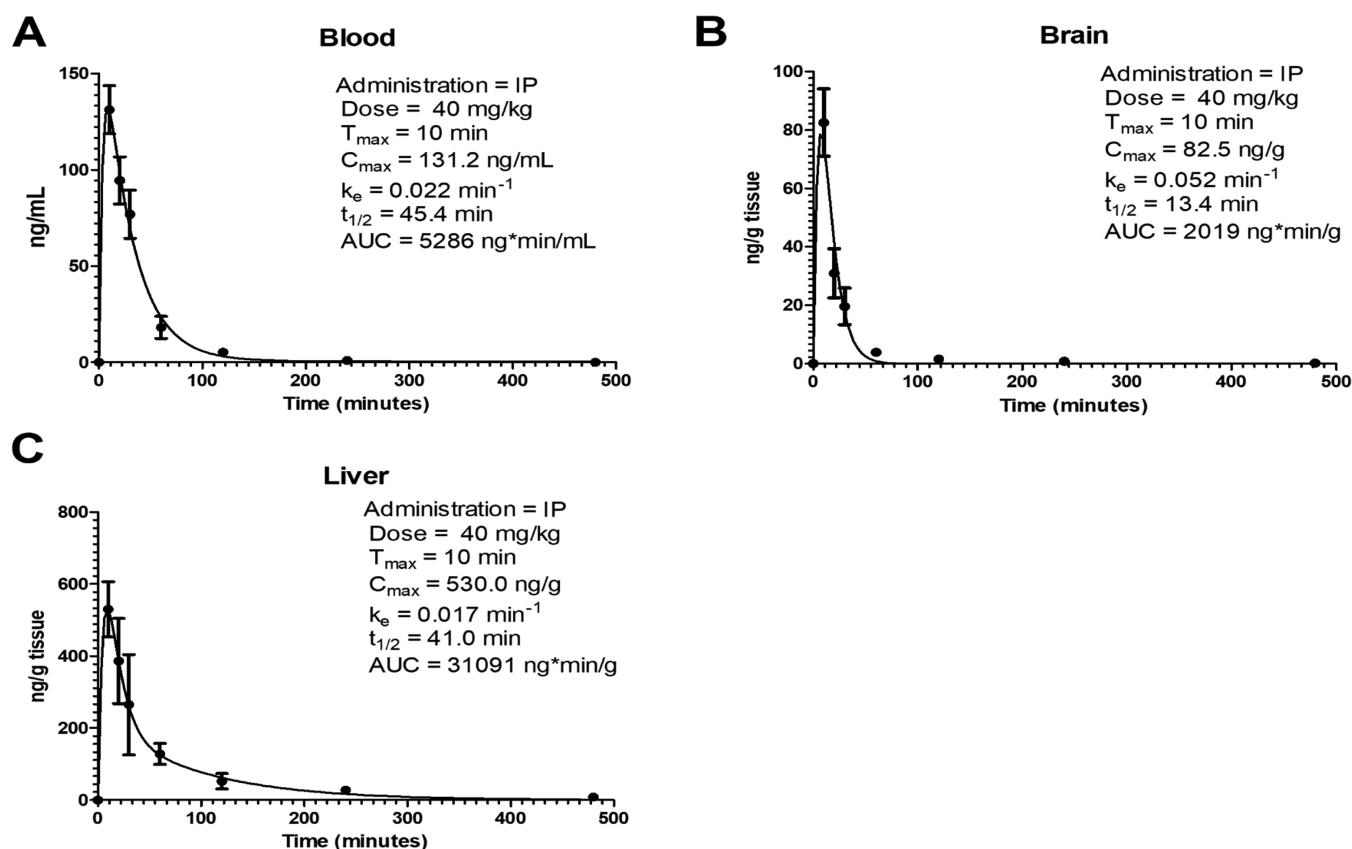


**Figure 5.** Pharmacokinetic analysis of MJM-1 in blood, brain, and liver. Swiss Webster mice were injected i.p. with 40 mg/kg MJM-1, and blood (A), brain (B), and liver (C) concentrations were determined by liquid chromatography–mass spectrometry (LC–MS/MS) at different time points. Data are depicted as a mean  $\pm$  SD ( $n = 4$ ) and fitted to a two-compartment pharmacokinetics (PK) model to determine PK parameters.

novel object. Because mice exhibit an inherent preference for novelty, those that spend more time than chance (15 s) with the novel or moved object are considered to display intact consolidation of memory for the training objects. Mice completed object placement testing followed by object recognition testing. Objects were counterbalanced across mice to account for any object preferences that might be expressed. Bouts of testing were separated by 2 weeks to ensure that any effects of drug treatment were dissipated before the next treatment. Multiple doses of MJM-1 enhanced spatial memory consolidation (Figure 6C). Although one-way

analyses of variance (ANOVAs) did not indicate significant between-group differences ( $F(4,78) = 1.134$ ;  $p = 0.3467$ ), one-sample  $t$ -tests that assess memory within each group revealed a differential pattern of spatial memory consolidation among the groups. Mice receiving the negative DMSO control did not spend significantly more time with the moved object than the chance value of 15 s ( $t(16) = 0.6857$ ,  $p > 0.05$ ;  $n = 17$ ), suggesting that this group exhibited impaired memory for object location. In contrast, mice receiving the positive control, NaBu, spent significantly more time than chance with the moved object ( $t(14) = 2.265$ ,  $p = 0.0399$ ;  $n = 15$ ), indicating

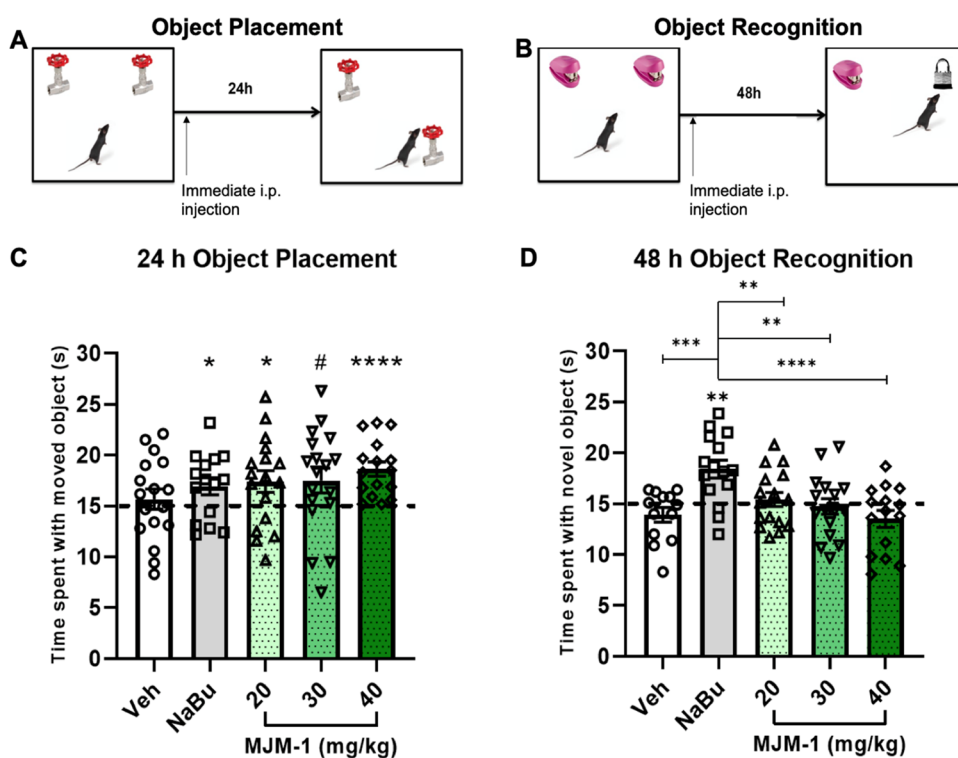


**Figure 6.** Post-training i.p. administration of MJM-1 enhances spatial, but not object recognition, memory in male mice. (A, B) Schematic of the object placement and object recognition tasks used to assess the consolidation of spatial memory and object recognition memory, respectively. See the text for a detailed description of task protocols. (C) Male mice receiving an i.p. injection of the HDACi sodium butyrate (NaBu), or 20 or 40 mg/kg of MJM-1 spent significantly more time than chance (dashed line at 15 s, \* $p < 0.05$ , \*\*\*\* $p < 0.0001$ ) with the moved object 24 h after training ( $n = 15$ – $18$ /group). Although not statistically significant, mice receiving the 30 mg/kg dose of MJM-1 displayed a strong trend toward spending more time than chance with the moved object ( $\#p = 0.0556$ ). (D) Only mice receiving NaBu treatment spent significantly more time than chance with the novel object 48 h after training (\*\* $p < 0.01$ , \*\*\* $p < 0.001$ ). Mice treated with NaBu also spent significantly more time with the novel object than every other treatment group (relative to NaBu) ( $n = 13$ – $15$ /group). Bars represent the mean  $\pm$  standard error of the mean (SEM).

enhanced memory for object location. Similarly, mice receiving 20 mg/kg MJM-1 ( $t(16) = 2.244$ ,  $p = 0.0393$ ;  $n = 17$ ) or 40 mg/kg MJM-1 ( $t(15) = 5.248$ ,  $p < 0.0001$ ;  $n = 16$ ) also spent significantly more time with the moved object than chance, indicating that these two doses of MJM-1 enhanced spatial memory consolidation. Although these increases may appear small, they are 12–24% greater than chance (15 s). Cohen's  $d$  for the  $t$ -tests indicates medium effect sizes for NaBu ( $d = 0.584$ ) and 20 mg/kg MJM-1 ( $d = 0.544$ ) and a large effect size for 40 mg/kg MJM-1 ( $d = 1.312$ ). Although not quite statistically significant, mice receiving 30 mg/kg MJM-1 also tended to spend more time than chance with the moved object ( $t(17) = 2.054$ ,  $p = 0.0556$ ;  $n = 18$ ). These results suggest that acute i.p. administration of MJM-1 can enhance spatial memory consolidation in male mice.

In contrast to its effects on spatial memory, MJM-1 did not influence object recognition memory consolidation (Figure 6D). One-sample  $t$ -tests indicated that mice receiving vehicle did not spend significantly more time than chance with the novel object ( $t(12) = 1.533$ ,  $p > 0.05$ ;  $n = 13$ ). Although mice receiving NaBu spent significantly more time than chance with the novel object, ( $t(14) = 3.915$ ,  $p = 0.0016$ ;  $n = 15$ ), those receiving the 20, 30, or 40 mg/kg MJM-1 did not ( $t(14-15) = 0.6089$ ,  $0.3235$ , and  $1.747$ , respectively,  $p > 0.05$ ;  $n = 15$ – $16$ ). The main effect of treatment was significant ( $F(4, 70) = 6.027$ ;  $p = 0.0003$ ), an effect driven by the fact that the NaBu-treated group differed significantly from every other treatment group

(NaBu vs Veh:  $p = 0.0002$ ; NaBu vs 20:  $p = 0.0077$ ; NaBu vs 30:  $p = 0.0013$ ; NaBu vs 40:  $p < 0.0001$ ). Taken together, these results indicate that MJM-1 can enhance spatial, but not object recognition, memory consolidation to a similar extent as the known memory-enhancing HDAC inhibitor NaBu.

## DISCUSSION

Although HDACis have established anticancer activity, this class of compounds has gained an intense interest in recent decades for its potential to alleviate memory loss in aging and neurodegenerative diseases like Alzheimer's disease (AD).<sup>37,38</sup> In preclinical studies, HDACis facilitate brain function and enhance memory formation and retention in wild-type rodents and mouse models of AD.<sup>26,39</sup> Although several well-known HDACis including SAHA, valproic acid, and trichostatin A are effective in treating CNS disorders such as Alzheimer's disease, brain cancer, and addiction,<sup>40</sup> their clinical application in this area has remained underdeveloped due to their limited ability to cross the BBB.<sup>18,31,41</sup> So far, researchers have discovered only a handful of analogues of HDAC inhibitors that can cross the BBB and have the potential to treat CNS disorders.<sup>31,42–44</sup> Considering the high efficacy of cyclic depsipeptide-type HDAC inhibitors as chemotherapeutic agents, we undertook a systematic approach to synthesize small disulfide molecules (Schemes 1 and 2), which could have high brain uptake as well as potency for memory formation. The successful synthesis of the desired compounds following the proposed scheme was

confirmed by our spectroscopic data, which include high-resolution mass spectrometry (HRMS),  $^{13}\text{C}$  NMR, and  $^1\text{H}$  NMR (see the Supporting Information).

In this study, we initially assessed whether MJM-1, our novel HDACi, could reduce cell viability. The MTT results demonstrate a dose-dependent behavior shown by MJM-1, where the treatment of 100 and 50  $\mu\text{M}$  reduced viability by  $\sim 80$  and  $\sim 50\%$ , respectively. The  $\text{LD}_{50}$  value of MJM-1 was approximately 40  $\mu\text{M}$ . Additional analogues of MJM-1 (MJM-2, MJM-3, MJM-4, MJM-5, MJM-6) were tested and showed no significant reduction in cellular proliferation at the highest dose tested (50  $\mu\text{M}$ ). Treatment with romidepsin in the nM range also showed a reduction of viability. This is consistent with previous studies testing romidepsin against prostate cancer cells.<sup>45</sup> Although romidepsin had a higher potency than our novel inhibitor, it has shown numerous clinical toxicities when used as an antineoplastic agent. Most commonly are hematological complications such as thrombocytopenia and anemia.<sup>46</sup>

Histone acetylation has been shown to play crucial roles in myriad biological processes including cell proliferation and carcinogenesis.<sup>47</sup> HDACs such as romidepsin have been shown to increase levels of acetylation in multiple tumor cells. Our immunofluorescence imaging results demonstrated high levels of histone acetylation in DU145 cells when treated with 100 and 50  $\mu\text{M}$  of MJM-1, which was less pronounced at the 25  $\mu\text{M}$  dose. Similarly, the treatment of DU145 cells with romidepsin in the nM range showed high levels of histone acetylation, which has been shown in previous studies.<sup>45</sup> The observed levels of histone acetylation after MJM-1 treatment were qualitatively lower than those after treatment with romidepsin, which could explain the lower toxicity exhibited by MJM-1, as shown in the MTD studies. Further assessment will include the quantification of acetylation levels using flow cytometry or mass spectrometry. *In vitro* studies supported the contention that decreased apparent cellular histone acetylation in the presence of MJM-1 results from HDAC inhibition (Figure 3F). Although several orders of magnitude less potent than romidepsin, MJM-1 inhibited all HDACs tested in a concentration-dependent fashion, and this activity is not restricted to class I HDACs. In addition, from the  $\text{IC}_{50}$  values (Table 1) of other MJM compounds, we observed that MJM-1 shows better or comparable HDAC inhibition.

To evaluate acute toxicity and assess potential safety, we determined the maximally tolerated dose (MTD).<sup>48</sup> The assay was performed in a way that conserved the compound and minimized the number of animals sacrificed during subsequent *in vivo* study. Both MJM-1 and SAHA were well tolerated during the study, and no significant loss of body weight or other signs of overt toxicity were observed. In contrast, morbidity and mortality were substantially higher with romidepsin. These data suggest a much more favorable safety profile for MJM-1, such that MJM-1 is far less toxic than romidepsin (even at a higher dose).

MJM-1 has a longer half-life in blood and liver than brain after i.p. administration. The elimination of MJM-1 may depend on its conversion to the corresponding thiol in a reductive environment, as well as metabolism and secretion. Levels of the thiol species, if present, were below detectable limits in blood after i.p. administration. Nevertheless, we think that the thiol is likely to be present because the prodrug MJM-1 can be detected or complexation of cations or the formation of mixed disulfides with, e.g., glutathione, complicated the

quantification of the thiol compound by MS/MS. The ability of MJM-1 to cross the BBB was supported by memory enhancement after i.p. injection and indicated by PK analysis. The  $C_{\text{max}}$  in the brain was 63% of the  $C_{\text{max}}$  in blood at 10 min. This confirms a rapid and robust BBB transit of MJM-1. Interestingly, the half-life of MJM-1 is significantly shorter in the brain than in blood or liver. Brain tissue is highly dependent on redox systems that support synaptic plasticity and neurotransmitter recycling.<sup>49</sup> If reduction to the thiol can be assumed a major metabolic pathway, then the local accumulation of thiol formed by MJM-1 may be greater in the brain than elsewhere. Finally, the AUC (liver) is almost 6-fold higher than the AUC (blood); thus, MJM-1 is compartmentalized in the liver, which might be due to the hydrophobic nature of MJM-1 (unspecific binding) or a specific interaction of unknown nature. The elimination rate in the liver is comparable to that in the blood; thus, accumulated MJM-1 in the liver is not rate-limiting for metabolism. Further research will identify the metabolites of MJM-1 *in vivo* and their approximate rates for formation in blood and the brain. These future studies will not only focus on phase I and phase II metabolism but also on the redox kinetics of these unique disulfides.

It has been reported that the physicochemical properties of small molecules correlate with their ability to cross the BBB. Several physicochemical properties are widely used to assess a compound's ability to cross the BBB, including lipophilicity (clogP), topological polar surface area (tPSA), and molecular weight (MW).<sup>50</sup> In general, CNS active drugs have molecular weights less than 450 g/mol, clogP values of 2–4, and tPSA values less than 90  $\text{\AA}^2$ .<sup>50</sup> The predicted values of these properties for MJM-1 and romidepsin were calculated by Chem Biodraw Ultra 12.0 software and have been compared. The calculated molecular weight of MJM-1 is 462.21 g/mol, the predicted clogP value is 4.0488, and the predicted tPSA value is 93.07  $\text{\AA}^2$ . These values are within or near those reported to be optimal for brain-penetrant drugs. On the other hand, the values for romidepsin are outside the range with an MW of 540.21 g/mol, a clogP of 3.4427, and a tPSA of 142.70  $\text{\AA}^2$ . The significant differences in their physicochemical properties may account for MJM-1's ability to penetrate BBB more effectively.

Furthermore, we quantified MJM-1 in the dorsal hippocampus, a brain region that mediates multiple forms of episodic memory, including spatial and object recognition memory<sup>51</sup> and that deteriorates in aging and neurodegenerative diseases.<sup>52,53</sup> These results are promising because they suggest that the memory-enhancing effects of MJM-1 are due to its presence in the dorsal hippocampus during the consolidation window of long-term memory formation. The consolidation window is a brief period of time following a learning event in which numerous molecular processes, such as gene transcription, support the transfer of initially labile information into long-term memory.<sup>54,55</sup> The consolidation phase for spatial and object recognition memory has been previously shown to last  $\sim 1$  h following training, a time frame that is amenable to the inhibitory effects of MJM-1.<sup>34,36</sup> Finally, we demonstrate that MJM-1 can enhance spatial memory consolidation in male mice. A single post-training i.p. injection of 20 or 40 mg/kg MJM-1, and to a lesser extent 30 mg/kg MJM-1, enhanced spatial memory consolidation in the object placement task. These findings also indicate that MJM-1 similarly enhances spatial memory consolidation to the

established HDACi NaBu. The spatial memory-enhancing effects of MJM-1 are consistent with a number of previously published studies utilizing extant HDACi in object placement tasks. For instance, post-training i.p. administration of NaBu has been previously shown to enhance spatial memory in male mice using a comparable object placement task.<sup>12</sup> Similarly, post-training infusion of NaBu or other HDACi, including MS-275 and TSA, directly into the dorsal hippocampus enhances object placement memory consolidation in male mice.<sup>14,56</sup> As such, the ability of MJM-1 to facilitate spatial memory formation is consistent with those of other well-established HDACis.

The spatial memory-enhancing effects of MJM-1 are consistent with our mass spectrometry analyses, demonstrating that the 40 mg/kg dose of MJM-1 can be detected in the dorsal hippocampus at both 10 and 30 min following i.p. injection. Although the lifetime of the drug in the dorsal hippocampus appears to be relatively short, memory consolidation occurs in this task within 90 min.<sup>57</sup> Thus, we observe spatial memory-enhancing effects of MJM-1 24 h later because MJM-1 is in the dorsal hippocampus during a critical window of time during which it can facilitate the transcription of genes critical for the consolidation of spatial information.<sup>7</sup>

We also demonstrate that MJM-1 inhibits both class I (HDAC1, 2, 3, 8) and class IIb HDACs (HDAC6) with similar potency. MJM-1 is a more potent inhibitor in the presence of a reducing agent, DTT. This suggests that MJM-1 compound is a prodrug that remains inactive and needs to be activated by reduction. Interestingly, this inhibitory profile is consistent with our observed beneficial effect on spatial memory formation. Previous studies have demonstrated that mice overexpressing HDAC2 exhibited impaired spatial memory formation,<sup>15</sup> whereas the focal deletion of HDAC3 within the dorsal hippocampus enhanced spatial but not object recognition, memory in male mice.<sup>16</sup> Furthermore, the deletion of HDAC6 rescued spatial memory impairments in a mouse model of AD.<sup>58</sup>

In contrast, our data also indicate that MJM-1 does not enhance object recognition memory consolidation. The lack of an effect on object recognition memory is inconsistent with other studies in which post-training i.p. injection of NaBu given to young or aged male rodents or dorsal hippocampal infusion of TSA given to young ovariectomized female mice enhances object recognition memory consolidation.<sup>11–13,59</sup> The reasons for this discrepancy are unclear at present. The object placement and recognition tasks are frequently used in the field of learning and memory because they are nonaversive, one-trial learning tasks that are amenable to the repeated use of pharmacological interventions.<sup>36</sup> However, the distinct molecular mechanisms that support the formation of spatial and object recognition memories remain unclear, let alone how HDACis interact within the existing molecular framework to enhance one form of learning over another.

The inconsistent effects of MJM-1 on spatial vs recognition memory may reflect distinct contributions of individual HDACs that support memory formation in a task-specific manner. For instance, mice that overexpress HDAC2, but not HDAC1, exhibited impaired spatial memory formation,<sup>15</sup> whereas the focal deletion of HDAC3 in the dorsal hippocampus enhanced spatial, but not object recognition, memory in male mice.<sup>16</sup> Therefore, MJM-1 may preferentially influence spatial memory by partially inhibiting the activity of class I HDAC2 and HDAC3. Alternatively, differential

regulation by MJM-1 of the histone acetyltransferase transcription factor/coactivator complex CREB (cAMP response element-binding protein) binding protein (CBP) may play a role, as post-training i.p. injection of NaBu enhances both spatial and object recognition memory in wild-type mice but only facilitates object recognition in CBP mutant mice.<sup>12</sup> Thus, spatial and object recognition memory may differ in their requirement for interactions with CREB: CBP proteins. Finally, the differential effects of MJM-1 on these two types of memory may relate to the brain circuitry that mediates them. Whereas spatial memory in rodents predominately relies on the hippocampus,<sup>60</sup> object recognition memory is involving the hippocampus, insular cortex, and multiple regions of the temporal lobe.<sup>61,62</sup> Interestingly, NaBu enhanced object recognition memory consolidation when it was infused post-training into the insular cortex but not the hippocampus, of male rats.<sup>56</sup> Although our mass spectrometry analyses indicated MJM-1 penetration into the hippocampus, it remains unclear whether MJM-1 localizes to and/or activates other brain regions that are relevant for object recognition memory formation.

Limitations of the study center around the fact that the cellular mechanism of action of MJM-1 is still unclear. Although MJM-1 was designed to be a brain-penetrant prodrug, only the prodrug form could be detected in the brain (Figure 5). *In vitro*, MJM-1 reduction enhances potency at least 100-fold, but this reduced form inhibits HDACs 1000 times less potently than romidepsin. Also, unlike romidepsin, MJM-1 displays little specificity for class I HDACs. Finally, only five other putative prodrugs were synthesized that resemble MJM-1. All inhibited HDAC2 with a similar potency as MJM-1 (Table 1), meaning that few structure–activity relationships can be gleaned from this study. To address these limitations, further SAR studies are underway.

## CONCLUSIONS

In conclusion, we have synthesized a novel nontoxic small-molecule HDACi that promotes histone acetylation, rapidly penetrates the blood–brain barrier, and enhances spatial but not object recognition memory in mice. As an HDAC inhibitor, MJM-1 significantly increased the amount of acetylated histone proteins present in tumor cells that correlated with cytotoxicity. Furthermore, the maximum tolerable dose determination assay established that MJM-1 has favorable tolerability compared to romidepsin. The ability of MJM-1 to enhance spatial memory consolidation in male mice suggests that this compound may represent a promising putative treatment for spatial memory deficits in humans. Future work should assess the effects of MJM-1 in other spatial memory tasks (e.g., the Morris water maze) to determine the extent to which MJM-1s memory-enhancing effects generalize to other tests of spatial memory. Moreover, because spatial memory impairments are characteristic of normal aging and neurodegenerative diseases such as Alzheimer's disease, and the hippocampus, which is largely responsible for spatial memory formation, is one of the first brain structures to deteriorate in Alzheimer's disease, future work should also examine the extent to which MJM-1 rescues spatial memory deficits in mouse models of aging and Alzheimer's. Such work should include female subjects as well, given the increased risks to women of developing Alzheimer's relative to men.

## EXPERIMENTAL SECTION

**Chemistry General.** All reactions were performed under a dry nitrogen atmosphere using standard Schlenk techniques unless otherwise noted. All reaction vessels were flame-dried under vacuum and filled with nitrogen prior to use. Reagents and solvents were purchased from Sigma-Aldrich, Milwaukee. All  $^1\text{H}$  and  $^{13}\text{C}$  NMR spectra were recorded in  $\text{CDCl}_3$  and  $\text{CD}_3\text{OD}$  (internal standard: 7.26 ppm, 1H; 77.16 ppm,  $^{13}\text{C}$ ) at room temperature with Bruker 300 MHz and 500 MHz spectrometers. The chemical shifts ( $\delta$ ) are given in parts per million (ppm), and the coupling constants are given in Hertz (Hz). The following abbreviations are used: s, singlet; d, doublet; t, triplet; q, quartet; and m, multiplet. Previously reported compounds were identified by  $^1\text{H}$  NMR. All new compounds were additionally characterized by  $^1\text{H}$  NMR,  $^{13}\text{C}$  NMR, and high-resolution mass spectrometry (HRMS). HRMS was obtained using the electrospray ionization (ESI) technique using quadrupole time-of-flight (LCMS-IT-TOF, Shimadzu Corporation). For column chromatography, silica gel (35–70  $\mu\text{m}$ ) was used. Thin-layer chromatography (TLC) was performed on aluminum-backed plates precoated (0.25 mm) with silica gel 60 F254 with a suitable solvent system and was visualized using UV fluorescence and/or iodine chamber. The preparative high-performance liquid chromatography (HPLC) (Shimadzu Corporation) was conducted with the column (Thermo Fisher, Prep-C18, 21.1  $\times$  150 mm, 10  $\mu\text{m}$ ) system. The purity of biologically tested compounds was >95%. Purity was evaluated by Shimadzu LCMS 2020 single quadrupole mass analyzer (Shimadzu, Kyoto, Japan) in electrospray ionization mode. The LC–MS was operated with a heat block temperature of 400  $^\circ\text{C}$ , a flow rate of 0.4 mL/min, a drying gas flow of 15 L/min, a desolvation line temperature of 250  $^\circ\text{C}$ , a nebulizing gas flow of 1.5 L/min, and both needle and interface voltages of 4.5 kV. The response acquisition was performed using LabSolutions software. The analytes were analyzed with a Pinnacle C18 column 100  $\times$  2.1 mm (Restek Corporation). The particle and pore size of the column were 3  $\mu\text{m}$  and 110  $\text{\AA}$ , respectively. Solvent A was  $\text{H}_2\text{O}$  with 0.1% formic acid and solvent B was 100% acetonitrile or methanol, and the ambient temperature was used as the column oven temperature.

**3-(Tritylthio)propanal<sup>63–65</sup> (3).** A round-bottom flask was charged with triphenylmethanethiol (5.0 g, 18.1 mmol), and contents were dissolved in dichloromethane (50 mL) under nitrogen. Triethylamine (3 mL, 21.7 mmol) and acrolein (1.2 mL, 18.1 mmol) were added consecutively to the mixture and was stirred for 2 h and then concentrated *in vacuo*. Upon completion, the crude product was purified by flash column chromatography with a 25% ethyl acetate/hexane solution until the product spot eluted. Product 3 was recrystallized with toluene and collected as a white solid (5.3 g, 88%).  $^1\text{H}$  NMR ( $\text{CDCl}_3$ , 500 MHz):  $\delta$  (ppm) 9.59 (s, 1H), 7.47 (d,  $J$  = 10.0 Hz, 6H), 7.47 (q,  $J$  = 7.5 Hz, 6H), 7.26 (t,  $J$  = 5.0 Hz, 3H), 2.51 (t,  $J$  = 7.5 Hz, 2H), 2.41 (t,  $J$  = 7.5 Hz, 2H);  $^{13}\text{C}$  NMR ( $\text{CDCl}_3$ , 125 MHz):  $\delta$  (ppm) 200.4, 144.5, 129.6, 128.0, 126.8, 67.0, 42.7, 24.4.

**(E)-5-(Tritylthio)pent-2-enal<sup>65</sup> (4).** A charged round-bottom flask containing 3-(tritylthio)propanal 3 (5.0 g, 15.0 mmol) and 2-(triphenylphosphoranylidene)acetaldehyde (5.3 g, 16.6 mmol) was put under nitrogen, and the contents of the flask were dissolved in benzene (100 mL) and then refluxed overnight. The concentrated crude product was purified via flash column chromatography with a 20% ethyl acetate/hexane solution and finally recrystallized with toluene to afford pure product 4 (3.8 g, 70%).  $^1\text{H}$  NMR ( $\text{CDCl}_3$ , 500 MHz):  $\delta$  (ppm) 9.46 (d,  $J$  = 7.8 Hz, 1H), 7.45 (dd,  $J$  = 5.2, 3.4 Hz, 6H), 7.32 (dd,  $J$  = 10.3, 4.9 Hz, 6H), 7.27–7.23 (m, 3H), 6.65 (dt,  $J$  = 15.6, 6.4 Hz, 1H), 6.00 (ddd,  $J$  = 15.7, 7.8, 1.3 Hz, 1H), 2.36 (m,  $J$  = 13.0, 6.6, 1.8 Hz, 4H);  $^{13}\text{C}$  NMR ( $\text{CDCl}_3$ , 125 MHz):  $\delta$  (ppm) 193.8, 155.8, 144.6, 133.7, 129.6, 128.0, 126.8, 67.0, 31.8, 30.1.

**(E)-tert-Butyl-3-hydroxy-7-(tritylthio)hept-4-enoate (6).** A round-bottom flask was charged with THF (50 mL) and cooled to  $-78$   $^\circ\text{C}$  under nitrogen. Later, diisopropylethylamine (DIPEA) (9.4 mL, 53.8 mmol) and *n*-butyllithium (21.5 mL, 53.8 mmol) were added dropwise at  $-78$   $^\circ\text{C}$  and was stirred for 1 h. *tert*-Butyl acetate (6.6 mL, 48.9 mmol) was added at  $-78$   $^\circ\text{C}$  and was allowed to stir for an

additional 1 h. Lastly, (*E*)-5-(tritylthio)pent-2-enal (3.5 g, 9.8 mmol) was added to the mixture and was stirred for 45 min at  $-78$   $^\circ\text{C}$ . The reaction was quenched with a saturated solution of  $\text{NH}_4\text{Cl}$  (25 mL) and then concentrated *in vacuo*. Then, dichloromethane was added to the aqueous mixture and extracted three times, then dried over anhydrous  $\text{Na}_2\text{SO}_4$ , and concentrated *in vacuo*. The residue was purified with flash column chromatography (ethyl acetate/hexane, 1:9) and collected as product 6 as a white solid (3.6 g, 78%).  $^1\text{H}$  NMR ( $\text{CDCl}_3$ , 500 MHz):  $\delta$  (ppm) 7.46 (d,  $J$  = 5.0 Hz, 6H), 7.32 (t,  $J$  = 7.5 Hz, 6H), 7.25 (t,  $J$  = 7.5 Hz, 3H), 5.64–5.58 (m, 1H), 5.45 (dd,  $J$  = 15.0, 5.0 Hz, 1H), 4.43 (s, 1H), 3.09 (s, 1H), 2.48–2.42 (m, 2H), 2.25 (t,  $J$  = 5.0 Hz, 2H), 2.13 (t,  $J$  = 7.0 Hz, 2H), 1.49 (s, 9H);  $^{13}\text{C}$  NMR ( $\text{CDCl}_3$ , 125 MHz):  $\delta$  (ppm) 171.8, 144.9, 132.1, 129.9, 129.6, 127.9, 126.6, 81.3, 68.7, 66.6, 42.4, 31.5, 31.4, 28.2. HRMS (ESI<sup>+</sup>): calculated ( $m/z$ ) for  $\text{C}_{30}\text{H}_{34}\text{O}_3\text{S}$  ( $M + \text{Na}$ )<sup>+</sup>: 497.2121, found 497.2129.

**(4E,4'E)-Di-tert-butyl-7,7'-disulfanediylbis(3-hydroxyhept-4-enoate) (MJM-1).** (*E*)-*tert*-Butyl-3-hydroxy-7-(tritylthio)hept-4-enoate 6 (1.0 g, 2.1 mmol) was dissolved in a 10:1 solution of  $\text{CH}_2\text{Cl}_2/\text{MeOH}$  (10 mL) and was added dropwise to the solution of iodine (0.27 g, 2.1 mmol) and sodium acetate (0.17 g, 0.464 mmol) in a 10:1 solution of  $\text{CH}_2\text{Cl}_2/\text{MeOH}$  (15 mL) at 0  $^\circ\text{C}$  under nitrogen. The mixture was allowed to stir for 2 h. The reaction was quenched by adding a saturated sodium thiosulfate ( $\text{Na}_2\text{S}_2\text{O}_3$ ) solution. The aqueous layer was extracted with dichloromethane (3  $\times$  15 mL) and then with ethyl acetate (3  $\times$  15 mL) and concentrated *in vacuo*. The concentrated crude product was first purified by column chromatography (ethyl acetate/hexane, 1:4). Then, this column purified product was injected in the HPLC (Shimadzu Corporation) with the column (Prep-C18, 21.2  $\times$  150 mm, 10  $\mu\text{m}$ ) system and 58% ACN/ $\text{H}_2\text{O}$  was used to elute through the column under a flow rate of 20 mL/min. The wavelength was set at 254 nm to detect and collected the pure compound MJM-1 at 7.60–11.00 min in a fraction collector (0.66 g, 68%).  $^1\text{H}$  NMR ( $\text{CDCl}_3$ , 300 MHz):  $\delta$  (ppm) 5.70–5.60 (m, 1H), 5.48 (dd,  $J$  = 15.0, 6.0 Hz, 1H), 4.38 (q,  $J$  = 6.0 Hz, 1H), 3.3 (s, 1H), 2.64 (t,  $J$  = 7.5 Hz, 2H), 2.38–2.31 (m, 4H), 1.38 (s, 9H);  $^{13}\text{C}$  NMR ( $\text{CDCl}_3$ , 125 MHz):  $\delta$  (ppm) 171.6, 132.8, 129.1, 81.2, 68.7, 42.5, 38.1, 31.8, 28.1. HRMS (ESI<sup>+</sup>): calculated ( $m/z$ ) for  $\text{C}_{22}\text{H}_{38}\text{O}_6\text{S}_2$  ( $M + \text{Na}$ )<sup>+</sup>: 485.2002, found 485.1995.

**(E)-3-Hydroxy-7-(tritylthio)hept-4-enoic Acid<sup>65</sup> (8).** Lithium hydroxide (3.0 g, 126.5 mmol) was added to a solution of (*E*)-*tert*-butyl-3-hydroxy-7-(tritylthio)hept-4-enoate 6 (3.0 g, 6.3 mmol), which was dissolved in a 4:1 ratio of THF/water (50 mL) and heated to 50  $^\circ\text{C}$ . After 12 h of stirring, the reaction was then diluted with water (20 mL) and then acidified to a pH of 4–5 with  $\text{KHSO}_4$ . The aqueous layer was extracted with ethyl acetate (20 mL) four times. The combined organic layers were then washed with water, brine, dried over anhydrous sodium sulfate, and concentrated *in vacuo*. Finally, the residue was purified with flash column chromatography (ethyl acetate/hexane, 9:10) to obtain product 8 as a white solid (2.5 g, 95%).  $^1\text{H}$  NMR ( $\text{CDCl}_3$ , 300 MHz):  $\delta$  (ppm) 7.43 (d,  $J$  = 6.0 Hz, 6H), 7.30 (t,  $J$  = 7.5 Hz, 6H), 7.25 (t,  $J$  = 6.0 Hz, 3H), 5.66–5.57 (m, 1H), 5.44 (dd,  $J$  = 15.0, 6.0 Hz, 1H), 4.48 (q,  $J$  = 6.0 Hz, 1H), 2.56 (d,  $J$  = 6.0 Hz, 2H), 2.25 (t,  $J$  = 7.5 Hz, 2H), 2.11 (q,  $J$  = 6.0 Hz, 2H);  $^{13}\text{C}$  NMR ( $\text{CDCl}_3$ , 75 MHz):  $\delta$  (ppm) 177.3, 144.9, 131.6, 130.7, 129.6, 127.9, 126.7, 68.5, 66.7, 41.3, 31.4, 31.3.

**(4E,4'E)-7,7'-Disulfanediylbis(3-hydroxyhept-4-enoic Acid) (MJM-2).** Prepared by following the same procedure used to synthesize compound MJM-1. The crude was purified with flash column chromatography on silica gel with 100% ethyl acetate and afforded the pure product MJM-2 (yield 70%).  $^1\text{H}$  NMR ( $\text{CD}_3\text{OD}$ , 300 MHz):  $\delta$  (ppm) 5.80–5.71 (m, 1H), 5.62 (dd,  $J$  = 15.0, 6.0 Hz, 1H), 4.48 (q,  $J$  = 6.0 Hz, 1H), 2.76 (t,  $J$  = 7.5 Hz, 2H), 2.49–2.43 (m, 4H);  $^{13}\text{C}$  NMR ( $\text{CD}_3\text{OD}$ , 75 MHz):  $\delta$  (ppm) 173.7, 133.3, 128.7, 68.6, 42.1, 37.7, 31.6. HRMS (ESI<sup>+</sup>): calculated ( $m/z$ ) for  $\text{C}_{14}\text{H}_{22}\text{O}_6\text{S}_2$  ( $M + \text{Na}$ )<sup>+</sup>: 373.07500, found 373.07478.

**(E)-N-(tert-Butyl)-3-hydroxy-7-(tritylthio)hept-4-enamide (10).** (*E*)-3-Hydroxy-7-(tritylthio)hept-4-enoic acid 8 (500 mg, 1.2 mmol) and tertiary butylamine (125  $\mu\text{L}$ , 1.2 mmol) were dissolved in anhydrous dichloromethane (15 mL) under nitrogen. Then, benzo

osbenzotriazol-1-yl-oxytripyrrolidinophosphonium hexafluorophosphate (PyBOP) (746 mg, 1.4 mmol) was added to the solution at 0 °C and stirred for 20 min. Then, DIPEA (832  $\mu$ L, 1.19 mmol) was added into the solution and the reaction was allowed to warm to 25 °C with continuous stirring for 12 h. It was then quenched with a saturated  $\text{NH}_4\text{Cl}$ , extracted with dichloromethane ( $3 \times 15$  mL), washed with brine, dried over  $\text{Na}_2\text{SO}_4$ , and then concentrated *in vacuo*. The residue was purified with column chromatography (hexane/ethyl acetate, 1:1) to afford compound **10** as a white solid (407 mg, 72%).  $^1\text{H}$  NMR ( $\text{CDCl}_3$ , 500 MHz):  $\delta$  (ppm) 7.43 (d,  $J = 10.0$  Hz, 6H), 7.30 (t,  $J = 7.5$  Hz, 6H), 7.23 (t,  $J = 7.5$  Hz, 3H), 5.66 (brs, 1H), 5.60–5.54 (m, 1H), 5.42 (dd,  $J = 15.0, 5.0$  Hz, 1H), 4.40 (t,  $J = 7.5$  Hz, 1H), 3.15, 3.92 (s, 1H), 2.31–2.21 (m, 4H), 2.12–2.07 (m, 2H), 1.35 (s, 9H);  $^{13}\text{C}$  NMR ( $\text{CDCl}_3$ , 125 MHz):  $\delta$  (ppm) 171.3, 144.9, 132.4, 129.7, 129.6, 127.9, 126.6, 69.3, 66.6, 51.4, 43.2, 31.5, 31.4, 28.8. HRMS (ESI<sup>+</sup>): calculated ( $m/z$ ) for  $\text{C}_{30}\text{H}_{35}\text{NO}_2\text{S}$  ( $M + \text{Na}$ )<sup>+</sup>: 496.22807, found 496.22851.

**(4E,4'E)-7,7'-Disulfaneyldibis(N-(tert-butyl)-3-hydroxyhept-4-enamide) (MJM-3)**. Prepared according to the procedure used to synthesize MJM-1. The crude was purified with column chromatography on silica gel (dichloromethane/methanol, 20:1) and obtained the pure product MJM-3 as a white solid (yield 68%).  $^1\text{H}$  NMR ( $\text{CDCl}_3$ , 500 MHz):  $\delta$  (ppm) 5.93 (s, 1H), 5.75–5.70 (m, 1H), 5.56 (dd,  $J = 15.0, 5.0$  Hz, 1H), 4.45 (s, 1H), 4.22 (s, 1H), 2.74 (t,  $J = 7.5$  Hz, 2H), 2.68 (q,  $J = 10.0$  Hz, 2H), 2.33–2.25 (m, 2H), 1.35 (s, 9H);  $^{13}\text{C}$  NMR ( $\text{CDCl}_3$ , 125 MHz):  $\delta$  (ppm) 171.4, 133.1, 129.0, 69.3, 51.4, 43.2, 38.3, 31.8, 28.8. HRMS (ESI<sup>+</sup>): calculated ( $m/z$ ) for  $\text{C}_{22}\text{H}_{40}\text{N}_2\text{O}_4\text{S}_2$  ( $M + \text{H}$ )<sup>+</sup>: 461.2502, found 461.2508.

**(E)-3-Hydroxy-N-phenyl-7-(tritylthio)hept-4-enamide (12)**. 1-Ethyl-3-(3-dimethylaminopropyl)carbodiimide (EDC) (82 mg, 53 mmol), 4-dimethylaminopyridine (DMAP) (86 mg, 0.12 mmol), and triethylamine (TEA) were consecutively added to the cooled (0 °C) solution of compound **8** (200 mg, 0.48 mmol) and aniline (45  $\mu$ L, 0.48 mmol) in anhydrous dichloromethane under nitrogen. The reaction was allowed to warm to 25 °C with continuous stirring for 12 h. It was then quenched with a saturated  $\text{NaHCO}_3$ , extracted with dichloromethane ( $3 \times 15$  mL), washed with brine, dried over  $\text{Na}_2\text{SO}_4$ , and then concentrated *in vacuo*. The residue was purified with column chromatography (hexane/ethyl acetate, 3:2) to afford compound **12** as a pure product (189 mg, 80%).  $^1\text{H}$  NMR ( $\text{CDCl}_3$ , 500 MHz):  $\delta$  (ppm) 7.96 (brs, 1H), 7.50 (d,  $J = 9.0$  Hz, 2H), 7.43 (d,  $J = 9.0$  Hz, 6H), 7.35–7.20 (m, 11H), 7.14 (d,  $J = 9.0$  Hz, 1H), 5.66–5.57 (m, 1H), 6.02 (dd,  $J = 15.0, 6.0$  Hz, 1H), 4.52 (s, 1H), 3.15 (s, 1H), 2.53 (t,  $J = 4.5$  Hz, 2H), 2.24 (t,  $J = 6.0$  Hz, 2H), 2.11 (t,  $J = 6.0$  Hz, 2H);  $^{13}\text{C}$  NMR ( $\text{CDCl}_3$ , 125 MHz):  $\delta$  (ppm) 169.9, 144.9, 137.6, 132.2, 130.5, 129.6, 129.0, 127.9, 126.7, 124.5, 120.1, 69.3, 66.7, 43.9, 31.4, 31.3. HRMS (ESI<sup>+</sup>): calculated ( $m/z$ ) for  $\text{C}_{32}\text{H}_{31}\text{NO}_2\text{S}$  ( $M + \text{Na}$ )<sup>+</sup>: 516.19677.2003, found 516.19679.

**(4E,4'E)-7,7'-Disulfaneyldibis(3-hydroxy-N-phenylhept-4-enamide) (MJM-4)**. Prepared according to the procedure used to synthesize compound MJM-1. The crude was purified with column chromatography on silica gel (dichloromethane/methanol, 50:1) and obtained the pure product MJM-4 as a white solid (yield 65.5%).  $^1\text{H}$  NMR ( $\text{CD}_3\text{OD}$ , 300 MHz):  $\delta$  (ppm) 7.55 (d,  $J = 6.0$  Hz, 2H), 7.31 (t,  $J = 7.5$  Hz, 2H), 7.10 (t,  $J = 7.5$  Hz, 1H), 5.81–5.71 (m, 1H), 5.64 (dd,  $J = 15.0, 6.0$  Hz, 1H), 4.56 (q,  $J = 6.0$  Hz, 1H), 2.68 (t,  $J = 7.5$  Hz, 2H), 2.56 (t,  $J = 7.5$  Hz, 2H), 2.41 (q,  $J = 6.0$  Hz, 2H);  $^{13}\text{C}$  NMR ( $\text{CD}_3\text{OD}$ , 75 MHz):  $\delta$  (ppm) 170.4, 138.3, 133.4, 128.9, 128.4, 123.8, 119.9, 69.2, 44.5, 37.7, 31.5. HRMS (ESI<sup>+</sup>): calculated ( $m/z$ ) for  $\text{C}_{26}\text{H}_{32}\text{N}_2\text{O}_4\text{S}_2$  ( $M + \text{Na}$ )<sup>+</sup>: 523.16957, found 523.16932.

**(2S)-Methyl-2-((E)-3-hydroxy-7-(tritylthio)hept-4-enamido)hexanoate<sup>66</sup> (14)**. **(E)-3-Hydroxy-7-(tritylthio)hept-4-enoic acid 8** (2.0 g, 4.8 mmol) and *D*-norleucine methyl ester hydrochloride salt (0.87 g, 4.8 mmol) were dissolved in anhydrous dichloromethane (50 mL) under nitrogen. Then, benzotriazol-1-yl-oxytripyrrolidinophosphonium hexafluorophosphate (PyBOP) (3.0 mg, 5.7 mmol) was added to the solution at 0 °C and stirred for 20 min. Then, DIPEA (3.3 mL, 19 mmol) was added into the solution and the reaction was allowed to warm to 25 °C and continued stirring for 12 h. It was then quenched with a saturated  $\text{NH}_4\text{Cl}$ , extracted with dichloromethane ( $3$

$\times 15$  mL), washed with brine, dried over  $\text{Na}_2\text{SO}_4$ , and then concentrated *in vacuo*. The residue was purified with column chromatography on silica gel (hexane/ethyl acetate, 3:2) to afford compound **14** as a white solid (2.2 g, 81%).  $^1\text{H}$  NMR ( $\text{CDCl}_3$ , 300 MHz):  $\delta$  (ppm) 7.43 (d,  $J = 10.0$  Hz, 6H), 7.30 (t,  $J = 7.5$  Hz, 6H), 7.24 (d,  $J = 10.0$  Hz, 3H), 6.43 (d,  $J = 5.0$  Hz, 1H), 5.62–5.56 (m, 1H), 5.45 (dd,  $J = 15.0, 5.0$  Hz, 1H), 4.64–4.60 (m, 1H), 4.44 (s, 1H), 3.76 (s, 3H), 3.50 (s, 1H), 2.45 (dd,  $J = 15.0, 5.0$  Hz, 1H), 2.37 (dd,  $J = 15.0, 10.0$  Hz, 1H), 2.24 (t,  $J = 7.5$  Hz, 2H), 2.11 (t,  $J = 5.0$  Hz, 1H), 1.87–1.83 (m, 1H), 1.68 (d,  $J = 5.0$  Hz, 1H), 1.33 (d,  $J = 5.0$  Hz, 4H), 0.92 (t,  $J = 7.5$  Hz, 3H);  $^{13}\text{C}$  NMR ( $\text{CDCl}_3$ , 75 MHz):  $\delta$  (ppm) 173.1, 171.5, 144.9, 132.2, 130.2, 129.6, 127.9, 126.6, 69.1, 66.6, 52.4, 52.1, 42.6, 32.1, 31.5, 31.4, 27.4, 22.3, 13.9.

**(2S,2'S)-Dimethyl-2,2'-((4E,4'E)-7,7'-disulfaneyldibis(3-hydroxyhept-4-enoyl))bis(azanedyll)dihexanoate (MJM-5)**. Prepared according to the procedure used to synthesize compound MJM-1. The crude was purified with column chromatography on silica gel with 100% ethyl acetate, and the pure product MJM-5 was obtained as a white solid (yield 75%).  $^1\text{H}$  NMR ( $\text{CDCl}_3$ , 500 MHz):  $\delta$  (ppm) 6.67 (d,  $J = 10.0$  Hz, 1H), 5.79–5.73 (m, 1H), 5.60 (dd,  $J = 15.0, 5.0$  Hz, 1H), 4.49 (q,  $J = 5.0$  Hz, 1H), 4.51 (s, 1H), 3.90 (brs, 1H), 3.75 (s, 3H), 2.74 (t,  $J = 7.5$  Hz, 2H), 2.51–2.41 (m, 4H), 1.88–1.81 (m, 1H), 1.71–1.65 (m, 1H), 1.35–1.28 (m, 4H), 0.89 (t,  $J = 7.5$  Hz, 3H);  $^{13}\text{C}$  NMR ( $\text{CDCl}_3$ , 125 MHz):  $\delta$  (ppm) 173.3, 171.8, 132.9, 129.3, 69.2, 52.4, 52.2, 42.9, 38.2, 31.8, 31.7, 27.5, 22.2, 13.8. HRMS (ESI<sup>+</sup>): calculated ( $m/z$ ) for  $\text{C}_{28}\text{H}_{51}\text{N}_2\text{O}_8\text{S}_2$  ( $M + \text{H}$ )<sup>+</sup>: 605.2925, found 605.2914.

**(2S)-2-((E)-3-Hydroxy-7-(tritylthio)hept-4-enamido)hexanoic Acid<sup>66</sup> (16)**. Prepared according to the procedure used to synthesize compound **8**. The residue was purified with column chromatography on silica gel (hexane/ethyl acetate, 1:1) to afford compound **16** as a white solid (yield 92%).  $^1\text{H}$  NMR ( $\text{CDCl}_3$ , 300 MHz):  $\delta$  (ppm) 7.43 (d,  $J = 10.0$  Hz, 6H), 7.30 (t,  $J = 7.5$  Hz, 6H), 7.24 (t,  $J = 7.5$  Hz, 3H), 6.68 (d,  $J = 5.0$  Hz, 1H), 6.57 (d,  $J = 5.0$  Hz, 1H), 5.61–5.56 (m, 1H), 5.47–5.41 (m, 1H), 4.57–4.44 (m, 1H), 4.46 (t,  $J = 10.0$  Hz, 1H), 2.46–2.36 (m, 2H), 2.23 (t,  $J = 7.5$  Hz, 2H), 2.10 (t,  $J = 10.0$  Hz, 1H), 1.91–1.87 (m, 1H), 1.72–1.68 (m, 1H), 1.35 (s, 4H), 1.29 (s, 1H), 0.92 (t,  $J = 5.0$  Hz, 3H);  $^{13}\text{C}$  NMR ( $\text{CDCl}_3$ , 75 MHz):  $\delta$  (ppm) 175.6, 172.3, 146.9, 144.9, 129.6, 127.9, 127.3, 126.7, 69.2, 66.7, 52.3, 42.7, 31.7, 31.5, 31.4, 27.4, 22.3, 13.9.

**(2S,2'S)-2,2'-((4E,4'E)-7,7'-Disulfaneyldibis(3-hydroxyhept-4-enoyl))bis(azanedyll)dihexanoic Acid (MJM-6)**. Prepared according to the procedure used to synthesize compound MJM-1. The crude was purified with column chromatography on silica gel (dichloromethane/methanol, 20:1), and the pure product MJM-6 (yield 84%) was obtained.  $^1\text{H}$  NMR ( $\text{CD}_3\text{OD}$ , 500 MHz):  $\delta$  (ppm) 5.80–5.71 (m, 1H), 5.62 (dd,  $J = 15.0, 5.0$  Hz, 1H), 4.45 (q,  $J = 7.5$  Hz, 1H), 4.27 (q,  $J = 3.0$  Hz, 1H), 3.76 (t,  $J = 7.5$  Hz, 2H), 2.45 (t,  $J = 7.5$  Hz, 4H), 1.85 (t,  $J = 7.5$  Hz, 1H), 1.68 (q,  $J = 6.0$  Hz, 1H), 1.36 (s, 4H), 0.93 (t,  $J = 3.0$  Hz, 3H);  $^{13}\text{C}$  NMR ( $\text{CD}_3\text{OD}$ , 125 MHz):  $\delta$  (ppm) 177.9, 171.4, 133.6, 128.5, 69.0, 54.9, 43.6, 37.7, 32.4, 31.6, 27.6, 22.3, 13.0. HRMS (ESI<sup>+</sup>): calculated ( $m/z$ ) for  $\text{C}_{26}\text{H}_{44}\text{N}_2\text{O}_8\text{S}_2$  ( $M + \text{H}$ )<sup>+</sup>: 577.2612, found 577.2610.

**Methods. Cell Culture.** The DU145 human prostate epithelial cell line (HTB-81) was purchased from ATCC (Manassas, VA). DU145 cells were cultured in Dulbecco's modified Eagle's medium (DMEM) (Life Technologies, Grand Island, NY), supplemented with 10% fetal bovine serum (FBS, Atlanta Biologicals, Flowery Branch, GA), 100 U/mL penicillin, 100  $\mu\text{g}/\text{mL}$  streptomycin, and 2 mM L-glutamine (all from ThermoFisher Scientific, Waltham, MA) in a humidified atmosphere at 37 °C and 5%  $\text{CO}_2$ . Cells were passaged using trypsin–ethylenediaminetetraacetic acid (EDTA) (ThermoFisher Scientific) when they reached 70% confluency.

**Cell Proliferation Assay.** DU145 cells were plated in 96-well microtiter plates (14 000 cells/well in 200  $\mu\text{L}$ ) and allowed to adhere for 24 h at 37 °C in 5%  $\text{CO}_2$ . Stock solutions (10 mM in DMSO) of MJM-1 and romidepsin (FK228, Selleckchem) were diluted in DMEM medium supplemented with 10% FBS to the desired concentration (100, 50, 25  $\mu\text{M}$  and 10, 5, 1.25 nM, respectively). An equivalent volume of DMSO in the medium was used as vehicle

control. Using a multichannel pipettor, the culture media was removed, and the compounds or vehicle control were added to the plate in triplicate. The plate was incubated as above for 48 h. Following incubation, the media was removed and 200  $\mu\text{L}$  of 250  $\mu\text{g}/\text{mL}$  3-(4,5-dimethylthiazol-2-yl)-2,5-diphenyltetrazolium bromide (MTT, Research Products International, Mount Prospect, IL) in DMEM was added to each well. Cells were incubated with the MTT solution as above for 4 h. The MTT solution was removed, and 200  $\mu\text{L}$  of DMSO was added to each well and the plate was mixed on a rotator for 10 min at room temperature. Each well was further mixed with a pipettor to ensure the MTT precipitate was completely dissolved. Plates were read at 570 nm with a reference wavelength at 690 nm on a Molecular Devices Versamax plate reader (San Jose, CA). Data are presented as mean  $\pm$  SEM unless stated otherwise. A two-tailed Student's *t*-test was performed, and statistical significance was determined at  $p \leq 0.05$ . Analysis and IC<sub>50</sub> calculations were conducted using GraphPad Prism8 (La Jolla, CA).

**H3 Acetylation Assay.** The human prostate cell line DU145 was cultured as described above. At confluency of 70% or less, cells were lifted, counted, and resuspended at  $5 \times 10^4$  cells/mL. One milliliter of the cell suspension was added to each well of a 24-well plate, and cells were allowed to adhere for 24 h at 37 °C with 5% CO<sub>2</sub>. Next, the media was removed and increasing concentrations of MJM-1 (25, 50, 100  $\mu\text{M}$ ), romidepsin (10 nM), or DMSO control, diluted in media, were added to the wells in duplicate. The cells were incubated for 24 h before labeling. Cells were fixed in 300  $\mu\text{L}$  of 4% paraformaldehyde for 10 min at room temperature (RT). Cells were then permeabilized in 300  $\mu\text{L}$  Tris-buffered saline supplemented with 0.1% Tween 20 and 1% bovine serum albumin (TBS-T/BSA) at 4 °C for 1 h. The TBS-T/BSA was removed, and 300  $\mu\text{L}$  of rabbit anti-acetyl-histone H3 (Lys9/Lys14) antibody (Cell Signaling Technology, Danvers, MA) at 1:2000 dilution in TBS-T/BSA was added to each well and incubated at 4 °C overnight. The primary antibody was removed, cells were washed with TBS-T/BSA, and 300  $\mu\text{L}$  of goat antirabbit IgG AlexaFluor 488 (Jackson ImmunoResearch, West Grove, PA) at 1:500 dilution in TBS-T/BSA was added to each well and incubated at 4 °C for 1.5 h. The secondary antibody was removed, cells were washed as above, and 300  $\mu\text{L}$  of DAPI (0.3  $\mu\text{g}/\text{mL}$ ) was added to each well and incubated in the dark at RT for 15 min. The DAPI solution was removed, cells were washed as above, and then fixed in 1.5% formaldehyde. The cells were analyzed using a Nikon Eclipse TE-2000U inverted fluorescence microscope (Nikon, Melville, New York). Images were captured with a CoolSNAP ES camera (Photometrics, Tucson, Arizona) and analyzed using MetaVue software (Molecular Devices, Sunnyvale, California). Images from a minimum of five random high-powered fields were captured and analyzed for each sample. Results are representative of three independent experiments.

**Histone Deacetylase Assays.** The ability of various compounds to inhibit the ability of HDACs to remove acetyl groups *in vitro* was monitored using the HDAC-Glo I/II assay and screening system (Promega, product #G6430). The substrate in this assay is an acetylated peptide coupled to a luciferase derivative, which reacts with a proprietary reagent to generate aminoluciferin only when deacetylated. The product, aminoluciferin, can then be detected by measuring luminescence (au, arbitrary units) using luciferase and ATP. Recombinant, purified HDACs were obtained from BPS Bioscience: HDAC1 (Catalogue #50051), HDAC2 (Catalogue #50002), HDAC3 (Catalogue #50051), HDAC6 (Catalogue #50046), and HDAC8 (Catalogue #50008). Each protein was diluted to the same concentration based on their calculated molar mass in "HDAC-Glo Buffer" (25 mM Tris-HCl, 137 mM NaCl, 2.7 mM KCl, 1% v/v Triton X-100, pH 8). Compounds were first activated by reducing them with dithiothreitol (DTT) for 20 min at 23 °C. For reduction, 0.5  $\mu\text{L}$  of 350 mM DTT [in dimethyl sulfoxide (DMSO)] was added to 99.5  $\mu\text{L}$  of a 1 mM romidepsin (DMSO) or 0.7  $\mu\text{L}$  of 350 mM DTT was added to 19.3  $\mu\text{L}$  of 10 mM MJM-1. These mixtures were then serially diluted in HDAC-Glo buffer, and 5  $\mu\text{L}$  of each compound dilution was added to 5  $\mu\text{L}$  of a diluted HDAC such that the final HDAC concentration was 0.5 nM in each well of a 384-

well microplate (Greiner). After incubating compounds and HDACs for 10 min, 10  $\mu\text{L}$  of the HDAC-Glo substrate/developing reagent mixture (prepared according to the manufacturer's protocol) was added to each well, and the plate was mixed on an orbital shaker. After another 40 min at room temperature (23 °C), luminescence was measured with a FLOstar Omega plate reader (BMG Labtech). Data were fitted, using GraphPad Prism (v6), to a four-parameter concentration-response equation ( $Y = \text{Bottom} + (\text{Top} - \text{Bottom}) / (1 + 10^{((\text{LogIC}_{50} - X) * \text{Hillslope}))}$ ) to estimate the concentration of each HDACi needed to inhibit the reaction by 50% (IC<sub>50</sub>). "Top" values were constrained to the activity observed in the absence of HDACi's (DMSO only controls), and the "bottom" value was constrained to the luminescence observed in the absence of HDAC (no enzyme controls). All reactions were performed in triplicate. Errors reported for IC<sub>50</sub> values span 95% confidence intervals for the nonlinear regression.

**Analytical Studies. Animals.** C57BL/5 and Balb/c (wild-type) mice were either purchased from Jackson Laboratories (Bar Harbor, ME) or bred in house in a specific pathogen-free barrier facility in the animal resource center at the University of Wisconsin-Milwaukee. Female and male mice from 8 to 12 weeks of age were used. During the study, a total of 38 mice were used. All animals were screened regularly for pathogens. Procedures were approved by the Animal Care and Use Committee of the University of Wisconsin-Milwaukee (IACUC: 20-21#54) following the National Institutes of Health Guide for the Care and Use of Animals.

**Drug Injection and Anesthesia.** MJM-1 was resuspended in DMSO on the days of the experiment. Mice were individually weighed for drug calculations, and the average body weight was 26 g. Mice were physically restrained by the scruff for i.p. injections. A dose of either 20 or 40 mg/kg of body weight of MJM-1 was injected into the right lower abdominal region. Following the veterinary recommendation, all mice were anesthetized using diluted isoflurane until the mouse was sedated and demonstrated a slowed breathing pattern.

**Maximum Tolerated Dose (MTD) Study.** Generally, the determination of MTD is performed in a way that conserves compound and minimizes the number of animals sacrificed. Each animal was initially weighed using a digital scale and then injected i.p. with the compounds (listed in Table 2). A single mouse was given a single i.p. dose of 200 mg/kg, body weight, a second mouse received a dose of 100 mg/kg, and a third mouse received a single dose of 50 mg/kg. The mice were observed and weighed every day for 8 days. They were euthanized if they lost more than 20% of their body weight or if there were other signs of overt toxicity. If none of the mice survived with the first three doses, the next three dose levels (25, 12.5, and 6.25 mg/kg) were tested in a similar manner. This process was repeated until a tolerated dose was found, and the MTD value was determined. The last testing was repeated once. This dose was then designated the MTD and was used to calculate the amount of material administered to mice during efficacy testing.

**Tissue Collection.** Isoflurane-anesthetized mice were placed on the dissection table in a lateral recumbent position for blood collection. The head was grasped, and the eyelids were retracted to create proptosis of the right eye. A heparinized capillary pipette was gently inserted into the medial canthus at a 45° angle and, with twisting motion, the retro-orbital sinus was punctured. Blood was collected into Eppendorf tubes, and volumes were recorded and stored at -80 °C until use. Mice were then euthanized by CO<sub>2</sub> asphyxiation, the abdomen was opened using scissors, and the liver was taken out, rinsed, and weighed. Following liver collection, the base of the skull was opened using lateral incisions and the whole brain was removed using a laboratory spatula. In other experiments, the dorsal hippocampus was dissected bilaterally on wet ice, weighed, and stored at -80 °C until sample preparation.

**Biological Sample Preparation to Detect MJM-1.** Blood samples were thawed on ice, vortexed for 10 s, and a 100  $\mu\text{L}$  aliquot was combined with 400  $\mu\text{L}$  cold acetonitrile. Samples were vortexed for 30 s and centrifuged at 16 000g for 10 min at 4 °C. The supernatant layer was then transferred into clean tubes and evaporated using a Speedvac

concentrator. The residue was reconstituted with 400  $\mu\text{L}$  of acetonitrile and spin-filtered through 0.22  $\mu\text{m}$  nylon centrifugal filter units (Costar). After reconstitution, the samples were diluted if needed and 4,5-diphenylimidazole was added as the instrument standard. The injection volume was 3  $\mu\text{L}$  (LC–MS/MS, Shimadzu 8040). Brain and liver tissue samples were thawed, weighed, and homogenized directly into 400 or 600  $\mu\text{L}$  acetonitrile, respectively, using a Cole Palmer LabGen 7B Homogenizer. Samples were centrifuged at 16 000g for 10 min at 4 °C. The supernatant was then spin-filtered through 0.22  $\mu\text{m}$  nylon centrifugal filter units (Costar) and evaporated using a Speedvac concentrator. After reconstitution with 100  $\mu\text{L}$  of acetonitrile for brain and liver, respectively, 4,5-diphenylimidazole was added after spin-filtration through 0.22  $\mu\text{m}$  nylon centrifugal filter unit. The injection volume was 3  $\mu\text{L}$  (LC–MS/MS, Shimadzu 8040). Brain tissue samples (hippocampus) were prepared by following the same procedure mentioned above for brain sample, and the injection volume was 5  $\mu\text{L}$  for mass spectrometer (LC–MS/MS, Shimadzu 8040) analysis (see the [Supporting Information](#)).

**Pharmacokinetics and LC–MS/MS Analysis.** Blood samples were thawed on ice, vortexed for 10 s, and a 200  $\mu\text{L}$  aliquot was added to 300  $\mu\text{L}$  of cold acetonitrile containing 55 ng/mL of instrument standard (4,5-diphenylimidazole). Brain and liver tissue samples were thawed, weighed, and homogenized directly into 400 or 600  $\mu\text{L}$  of cold acetonitrile containing 13.75 or 27.5 ng/mL of the instrument standard (4,5-diphenylimidazole), respectively, using a Cole Palmer LabGen 7B Homogenizer. Samples were vortexed for 30 s and centrifuged at 14 000 rpm for 10 min. Next, the supernatant layer was spin-filtered through a 0.22  $\mu\text{m}$  nylon membrane centrifugal filter unit (Costar) and evaporated using a Speedvac concentrator. For blood, brain, and liver samples, the residues were reconstituted with 300, 100, and 300  $\mu\text{L}$  of acetonitrile, respectively, and spin-filtered through 0.22  $\mu\text{m}$  nylon centrifugal filter units (Costar). The injection volume was 5  $\mu\text{L}$  for mass spectrometer (LC–MS/MS, Shimadzu 8040) analysis. Separation was accomplished using a Pinnacle C18 column (100  $\times$  2.1 mm, particle and pore size are 3  $\mu\text{m}$  and 110 Å, respectively, Restek Corporation) under a flow rate of 0.5 mL/min, a column temperature at 40 °C, with 254 nm UV detection, a mobile phase of 0.1% formic acid (v/v) containing water (A) and MeCN (B), and a gradient time program of the following: 30% B (0)  $\rightarrow$  30% MeCN (0.5 min)  $\rightarrow$  75% B (5.0 min)  $\rightarrow$  99% MeCN (5.30 min), hold at 99% B (6.30 min), return to 35% B (6.80 min), hold at 35% B (9.0 min). Analytes were monitored under a positive mode using electrospray ionization (ESI). The following transitions were monitored in multiple reaction monitoring (MRM) modes for MJM-1:  $m/z$  485 [M + Na<sup>+</sup>] > 373.00,  $m/z$  485 [M + Na<sup>+</sup>] > 429.00,  $m/z$  485 [M + Na<sup>+</sup>] > 311.00; and for DPI:  $m/z$  221 > 193.00,  $m/z$  221 > 167.00,  $m/z$  221 > 152.00. The collision energy was optimized for each transition to obtain optimal sensitivity. The mass spectrometer was operated with a heat block temperature of 400 °C, a drying gas flow of 15 L/min, a desolvation line temperature of 250 °C, a nebulizing gas flow of 1.5 L/min, and both needle and interface voltages of 4.5 kV. The response acquisition was performed using LabSolutions software.

**Memory Studies. Animals.** Male C57BL/6 mice were obtained from Taconic Biosciences (Germantown, NY) at 10 weeks of age and housed individually in shoebox cages in a room (22–23 °C) with a 12/12 h light–dark cycle. During the study, a total of 89 mice were used. Food and water were provided *ad libitum*. Mice were handled for 30 s each for 3 consecutive days before behavioral testing. All procedures were conducted from 10:00 to 17:00 h in a dimly lit quiet room, and experimenters conducting behavioral testing were blind to the treatment each mouse received. All procedures were approved by the University of Wisconsin–Milwaukee Institutional Animal Care and Use Committee following the National Institutes of Health Guide for the Care and Use of Animals.

**Drugs and Injections.** All drugs were prepared the day of use and administered by a single intraperitoneal (i.p.) injection at a volume of 5 mL/kg immediately following behavioral training. The negative control (“vehicle”) treatment was 100% dimethyl sulfoxide (DMSO).

As a positive control, the nonselective HDACi sodium butyrate (NaBu) was dissolved in sterile saline to a concentration of 120 mg/mL for a dose of 600 mg/kg. This dose of NaBu previously enhanced object recognition memory consolidation in male mice.<sup>11</sup> MJM-1 was dissolved in 100% DMSO to a concentration of 8 mg/mL, for the 40 mg/mL dose, and then serially diluted to concentrations of 6 and 4 mg/mL for doses of 30 and 20 mg/kg, respectively. These doses were chosen based on our finding that both the 40 and 20 mg/kg doses of MJM-1 can be detected in the mouse DH 10 min following a single i.p. injection.

**Memory Testing.** The memory-enhancing effects of MJM-1 were examined using the object placement (OP) and object recognition (OR) tasks, which assess spatial memory and object recognition memory, respectively. Both tasks were performed as the Frick lab has described previously.<sup>34,35,67</sup> Briefly, OP and OR were conducted in a white open field box (width, 60 cm; length, 60 cm; height, 47 cm). Before training, mice were handled for 1 min/day for 3 consecutive days to acclimate mice to being held. On the second day of handling, a single Lego Duplo block was placed in the home cage to acclimate mice to objects. The Lego Duplo block was removed from the cage just prior to training. Following handling, mice underwent a single habituation session for 5 min/day for 2 consecutive days. During habituation, mice were allowed to move freely in the box without objects present.

On the training day, mice were habituated to the box for 2 min without objects present. They were then placed back into their home cage while the training objects were placed in the upper right- and left-hand corners of the box. Mice were then returned to the box and allowed to explore until they had accumulated a total of 30 s of exploration time with the objects (or until 20 min had elapsed). Experimenters manually scored in real time the duration of object exploration using ANYmaze tracking software (Stoelting). Object exploration was recorded when the mouse’s nose and/or front paws were directed toward and/or touching an object. Different objects were used for OP and OR, and all objects used were counterbalanced across mice to account for any potential object preferences. Immediately following training, mice received an i.p. injection of either vehicle, NaBu, or one of three doses of MJM-1 (20, 30, or 40 mg/kg) and were then returned to their home cage. All treatments were administered immediately post-training to pinpoint the effects of MJM-1 on the consolidation phase of memory formation. If mice did not accumulate 30 s of exploration time during training, they were then retrained 4–7 days later with different objects. Testing in OP and OR occurred 24 and 48 h post-training, respectively. These time points were chosen based on the previous evidence that vehicle-treated male mice no longer remember the location or identity of the objects at these time points.<sup>68</sup> Similarly, male mice can remember object identity 24 h after OR training.<sup>69,70</sup> During OP testing, the least-explored training object was moved to the lower right- or left-hand corner of the box. During OR testing, the least-explored training object was replaced with a novel object. Mice were given 20 min to accumulate 30 s of exploration time during both OP and OR testing. Because mice inherently prefer novelty, mice that remember the location and identity of the training objects should spend more time than chance (15 s) with the moved object in OP and the novel in OR. Chance is designated at 15 s because this value represents the equal exploration of both objects.<sup>69</sup> If mice did not accumulate 30 s of exploration time, then they were retrained no more than three times to successfully complete the OP and OR tasks. All mice were given at least 1 week between bouts of testing to ensure that any acute effects of previous drug injections dissipate before the next treatment.

**Memory Data Analyses.** Statistical analyses were conducted using GraphPad Prism8 (La Jolla, CA). For each behavioral experiment, separate one-sample *t*-tests were performed for each group to determine if the time spent with the novel object differs from chance (15 s).<sup>35,67–71</sup> This analysis assesses learning within a group. To assess differences between treatment groups, one-way analyses of variance (ANOVAs) were conducted for each task, followed by Fisher’s LSD post hoc tests. To ensure that post-training treatments do not influence activity during testing, the time for each mouse to

accumulate 30 s of exploration was collected and analyzed using one-way ANOVAs. Statistical significance was determined at  $p \leq 0.05$ .

## ■ ASSOCIATED CONTENT

### SI Supporting Information

The Supporting Information is available free of charge at <https://pubs.acs.org/doi/10.1021/acs.jmedchem.1c01928>.

NMR of all synthesized compounds and HRMS of new compounds, mass spectrometer analysis parameter, HPLC parameter, and traces of lead compound (PDF)  
Molecular string files for all of the synthesized compounds (CSV)

## ■ AUTHOR INFORMATION

### Corresponding Authors

Douglas A. Steeber – Department of Biological Sciences, University of Wisconsin-Milwaukee, Milwaukee, Wisconsin 53211, United States; Email: [steeber@uwm.edu](mailto:steeber@uwm.edu)

Karyn M. Frick – Department of Psychology, University of Wisconsin-Milwaukee, Milwaukee, Wisconsin 53211, United States; Email: [frickk@uwm.edu](mailto:frickk@uwm.edu)

M. Mahmud Hossain – Department of Chemistry and Biochemistry and Milwaukee Institute for Drug Discovery, University of Wisconsin-Milwaukee, Milwaukee, Wisconsin 53211, United States; [orcid.org/0000-0002-0874-4480](https://orcid.org/0000-0002-0874-4480); Email: [mahmun@uwm.edu](mailto:mahmun@uwm.edu)

### Authors

Jawad B. Belayet – Department of Chemistry and Biochemistry and Milwaukee Institute for Drug Discovery, University of Wisconsin-Milwaukee, Milwaukee, Wisconsin 53211, United States

Sarah Beamish – Department of Psychology, University of Wisconsin-Milwaukee, Milwaukee, Wisconsin 53211, United States

Mizzanoor Rahaman – Department of Chemistry and Biochemistry and Milwaukee Institute for Drug Discovery, University of Wisconsin-Milwaukee, Milwaukee, Wisconsin 53211, United States

Samer Alanani – Department of Biological Sciences, University of Wisconsin-Milwaukee, Milwaukee, Wisconsin 53211, United States

Rajdeep S. Virdi – Department of Chemistry and Biochemistry and Milwaukee Institute for Drug Discovery, University of Wisconsin-Milwaukee, Milwaukee, Wisconsin 53211, United States

David N. Frick – Department of Chemistry and Biochemistry and Milwaukee Institute for Drug Discovery, University of Wisconsin-Milwaukee, Milwaukee, Wisconsin 53211, United States; [orcid.org/0000-0002-2434-7223](https://orcid.org/0000-0002-2434-7223)

A. F. M. Towheedur Rahman – Department of Chemistry and Biochemistry and Milwaukee Institute for Drug Discovery, University of Wisconsin-Milwaukee, Milwaukee, Wisconsin 53211, United States

Joseph S. Ullicki – Department of Chemistry and Biochemistry and Milwaukee Institute for Drug Discovery, University of Wisconsin-Milwaukee, Milwaukee, Wisconsin 53211, United States

Sreya Biswas – Department of Biological Sciences, University of Wisconsin-Milwaukee, Milwaukee, Wisconsin 53211, United States

Leggy A. Arnold – Department of Chemistry and Biochemistry and Milwaukee Institute for Drug Discovery,

University of Wisconsin-Milwaukee, Milwaukee, Wisconsin 53211, United States; [orcid.org/0000-0003-1411-1572](https://orcid.org/0000-0003-1411-1572)

M. S. Rashid Roni – Department of Chemistry and Biochemistry and Milwaukee Institute for Drug Discovery, University of Wisconsin-Milwaukee, Milwaukee, Wisconsin 53211, United States; [orcid.org/0000-0002-3105-0540](https://orcid.org/0000-0002-3105-0540)

Eric Y. Cheng – College of Pharmacy, University of North Texas Health Science Center at Fort Worth, Fort Worth, Texas 76107, United States; [orcid.org/0000-0001-9336-2593](https://orcid.org/0000-0001-9336-2593)

Complete contact information is available at: <https://pubs.acs.org/doi/10.1021/acs.jmedchem.1c01928>

### Author Contributions

<sup>†</sup>J.B.B., S.B., M.R., and S.A. contributed equally to this work.

### Notes

The authors declare no competing financial interest.

## ■ ACKNOWLEDGMENTS

The authors would like to thank Brian Spindler and Dan Murphy for their assistance with compound synthesis, Kayla Simanek, Meredith Frank, and Jessye Hale for assistance with culture experiments, and Sarah M. Philippi for her assistance with memory testing. This project was supported by UWM Research Foundation/Bradley Catalyst grants to M.M.H. and K.M.F., as well as the University of Wisconsin-Milwaukee College of Letters and Science. This project was also funded by the TAP grant (Therapeutic Acceleration Program) Medical College of Wisconsin. K.M.F. and S.B.B. were additionally supported by the National Institutes of Health (R01MH107886, R15GM118304) and the Alzheimer's Association (SAGA-17-419092). D.A.S. and S.A. were supported, in part, by an award from the Chancellor's Office of the University of Wisconsin-Milwaukee. In addition, this work was supported by grant CHE-1625735 from the National Science Foundation, Division of Chemistry.

## ■ ABBREVIATIONS USED

AD, Alzheimer's disease; BBB, blood-brain barrier; CNS, central nervous system; DPI, 4,5-diphenylimidazole; DH, dorsal hippocampus; FK228, rhomidepsin; H3, histone 3; HDAC, histone deacetylase; HDACi, HDAC inhibitor; HPLC, high-performance liquid chromatography; i.p., systemic intraperitoneal injection; LC-MS, liquid chromatography-mass spectrometry; LDA, lithium diisopropylamide; MS-275, entinostat; MTT, 3-(4,5-dimethylthiazol-2-yl)-2,5-diphenyltetrazolium bromide; NaBu, sodium butyrate; *n*-BuLi, *n*-butyl lithium; OP, object placement; OR, object recognition; SAHA, vorinostat; TSA, trichostatin A; ZBG, zinc-binding group

## ■ REFERENCES

- (1) Alberini, C. M.; Kandel, E. R. The Regulation of Transcription in Memory Consolidation. *Cold Spring Harbor Perspect. Biol.* **2015**, *7*, No. a021741.
- (2) Grunstein, M. Histone Acetylation in Chromatin Structure and Transcription. *Nature* **1997**, *389*, 349–352.
- (3) Bannister, A. J.; Kouzarides, T. Regulation of Chromatin by Histone Modifications. *Cell Res.* **2011**, *21*, 381–395.
- (4) Lubin, F. D.; Roth, T. L.; Sweatt, J. D. Epigenetic Regulation of *bdnf* Gene Transcription in the Consolidation of Fear Memory. *J. Neurosci.* **2008**, *28*, 10576–10586.
- (5) Fortress, A. M.; Kim, J.; Poole, R. L.; Gould, T. J.; Frick, K. M. 17 $\beta$ -Estradiol Regulates Histone Alterations Associated with Memory

Consolidation and Increases Bdnf Promoter Acetylation in Middle-Aged Female Mice. *Learn. Mem.* **2014**, *21*, 457–467.

(6) Fischer, A.; Sananbenesi, F.; Mungenast, A.; Tsai, L.-H. Targeting the Correct HDAC(s) to Treat Cognitive Disorders. *Trends Pharmacol. Sci.* **2010**, *31*, 605–617.

(7) Gräff, J.; Tsai, L.-H. The Potential of HDACi as Cognitive Enhancers. *Annu. Rev. Pharmacol. Toxicol.* **2013**, *53*, 311–330.

(8) Broide, R. S.; Redwine, J. M.; Aftahi, N.; Young, W.; Bloom, F. E.; Winrow, C. J. Distribution of Histone Deacetylases 1–11 in the Rat Brain. *J. Mol. Neurosci.* **2007**, *31*, 47–58.

(9) Schmauss, C. The Roles of Class I Histone Deacetylases (HDACs) in Memory, Learning, and Executive Cognitive Functions: A Review. *Neurosci. Biobehav. Rev.* **2017**, *83*, 63–71.

(10) Vecsey, C. G.; Hawk, J. D.; Lattal, K. M.; Stein, J. M.; Fabian, S. A.; Attner, M. A.; Cabrera, S. M.; McDonough, C. B.; Brindle, P. K.; Abel, T.; Wood, M. A. Histone Deacetylase Inhibitors Enhance Memory and Synaptic Plasticity via CREB:CBP-Dependent Transcriptional Activation. *J. Neurosci.* **2007**, *27*, 6128–6140.

(11) Stefanko, D. P.; Barrett, R. M.; Ly, A. R.; Reolon, G. K.; Wood, M. A. Modulation of Long-Term Memory for Object Recognition via HDAC Inhibition. *Proc. Natl. Acad. Sci. U.S.A.* **2009**, *106*, 9447–9452.

(12) Haettig, J.; Stefanko, D. P.; Multani, M. L.; Figueroa, D. X.; McQuown, S. C.; Wood, M. A. HDAC Inhibition Modulates Hippocampus-Dependent Long-Term Memory for Object Location in a CBP-Dependent Manner. *Learn. Mem.* **2011**, *18*, 71–79.

(13) Zhao, Z.; Fan, L.; Frick, K. M. Epigenetic Alterations Regulate Estradiol-Induced Enhancement of Memory Consolidation. *Proc. Natl. Acad. Sci. U.S.A.* **2010**, *107*, 5605–5610.

(14) Hawk, J. D.; Florian, C.; Abel, T. Post-Training Intra-hippocampal Inhibition of Class I Histone Deacetylases Enhances Long-Term Object-Location Memory. *Learn. Mem.* **2011**, *18*, 367–370.

(15) Guan, J.-S.; Haggarty, S. J.; Giacometti, E.; Dannenberg, J.-H.; Joseph, N.; Gao, J.; Nieland, T. J. F.; Zhou, Y.; Wang, X.; Mazitschek, R.; Bradner, J. E.; et al. HDAC2 Negatively Regulates Memory Formation and Synaptic Plasticity. *Nature* **2009**, *459*, 55–60.

(16) McQuown, S. C.; Barrett, R. M.; Matheos, D. P.; Post, R. J.; Rogge, G. A.; Alenghat, T.; Mullican, S. E.; Jones, S.; Rusche, J. R.; Lazar, M. A.; Wood, M. A. HDAC3 Is a Critical Negative Regulator of Long-Term Memory Formation. *J. Neurosci.* **2011**, *31*, 764–774.

(17) Roper, S.; Esteller, M. The Role of Histone Deacetylases (HDACs) in Human Cancer. *Mol. Oncol.* **2007**, *1*, 19–25.

(18) Hanson, J. E.; La, H.; Plise, E.; Chen, Y. H.; Ding, X.; Hanania, T.; Sabath, E. V.; Alexandrov, V.; Brunner, D.; Leahy, E.; Steiner, P.; Liu, L.; Searce-Levie, K.; Zhou, Q. SAHA Enhances Synaptic Function and Plasticity In vitro but has Limited Brain Availability In vivo and does not Impact Cognition. *PLoS One* **2013**, *8*, No. e69964.

(19) Fennin, M. S.; Donigan, J. R.; Cohen, A.; Richon, V. M.; Rifkind, R. A.; Marks, P. A.; Breslow, R.; Pavletich, N. P. Structures of a Histone Deacetylase Homologue Bound to the TSA and SAHA Inhibitors. *Nature* **1999**, *401*, 188–193.

(20) Vannini, A.; Volpari, C.; Filocamo, G.; Casavola, E. C.; Brunetti, M.; Renzoni, D.; Chakravarty, P.; Paolini, C.; De Francesco, R.; Gallinari, P.; et al. Crystal Structure of a Eukaryotic Zinc-Dependent Histone Deacetylase, Human HDAC8, Complexed with a Hydroxamic Acid Inhibitor. *Proc. Natl. Acad. Sci. U.S.A.* **2004**, *101*, 15064–15069.

(21) Bertrand, P. Inside HDAC with HDACi. *Eur. J. Med. Chem.* **2010**, *45*, 2095–2116.

(22) Patil, V.; Guerrant, W.; Chen, P. C.; Gryder, B.; Benicewicz, D. B.; Khan, S. I.; Tekwani, B. L.; Oyelere, A. K. Antimalarial and Antileishmanial Activities of Histone Deacetylase Inhibitors with Triazole-Linked Cap Group. *Bioorg. Med. Chem.* **2010**, *18*, 415–425.

(23) Marson, C. M. Histone Deacetylase Inhibitors: Design, Structure-Activity Relationships and Therapeutic Implications for Cancer. *Anti-Cancer Agents Med. Chem.* **2009**, *9*, 661–692.

(24) Yoon, S.; Eom, G. H. HDAC and HDAC Inhibitor: From Cancer to Cardiovascular Diseases. *Chonnam Med. J.* **2016**, *52*, 1–11.

(25) Moore, D. Panobinostat (Farydak): A Novel Option for the Treatment of Relapsed or Relapsed and Refractory Multiple Myeloma. *Pharm. Ther.* **2016**, *41*, 296–300.

(26) Xu, K.; Dai, X.-L.; Huang, H.-C.; Jiang, Z.-F. Targeting HDACs: A Promising Therapy for Alzheimer's Disease. *Oxid. Med. Cell. Longevity* **2011**, *2011*, No. 143269.

(27) Sharma, S.; Taliyan, R. Targeting Histone Deacetylases: A Novel Approach in Parkinson's Disease. *Parkinson's Dis.* **2015**, *2015*, No. 303294.

(28) Mei, S.; Ho, A. D.; Mahlknecht, U. Role of Histone Deacetylase Inhibitors in the Treatment of Cancer (Review). *Int. J. Oncol.* **2004**, *25*, 1509–1519.

(29) Furumai, R.; Matsuyama, A.; Kobashi, N.; Lee, K.-H.; Nishiyama, M.; Nakajima, H.; Tanaka, A.; Komatsu, Y.; Nishino, N.; Yoshida, M.; Horinouchi, S. FK228 (Depsipeptide) as a Natural Prodrug That Inhibits Class I Histone Deacetylases. *Cancer Res.* **2002**, *62*, 4916–4921.

(30) Iwamoto, F. M.; Lamborn, K. R.; Kuhn, J. G.; Wen, P. Y.; Yung, W. K. A.; Gilbert, M. R.; Chang, S. M.; Lieberman, F. S.; Prados, M. D.; Fine, H. A. A Phase I/II Trial of the Histone Deacetylase Inhibitor Romidepsin for Adults with Recurrent Malignant Glioma: North American Brain Tumor Consortium Study 03-03. *Neurooncology* **2011**, *13*, 509–516.

(31) Seo, Y. J.; Kang, Y.; Muench, L.; Reid, A.; Caesar, S.; Jean, L.; Wagner, F.; Holson, E.; Haggarty, S. J.; Weiss, P.; King, P.; Carter, P.; Volkow, N. D.; Fowler, J. S.; Hooker, J. M.; Kim, S. W. Image-guided Synthesis Reveals Potent Blood-brain Barrier Permeable Histone Deacetylase Inhibitors. *ACS Chem. Neurosci.* **2014**, *5*, 588–596.

(32) Hiranaka, S.; Tega, Y.; Higuchi, K.; Kurosawa, T.; Deguchi, Y.; Arata, M.; Ito, A.; Yoshida, M.; Nagaoka, Y.; Sumiyoshi, T. Design, Synthesis, and Blood-Brain Barrier Transport Study of Pyrillamine Derivatives as Histone Deacetylase Inhibitors. *ACS Med Chem Lett.* **2018**, *9*, 884–888.

(33) Yurek-George, A.; Cecil, A. R. L.; Mo, A. H. K.; Wen, S.; Rogers, H.; Habens, F.; Maeda, S.; Yoshida, M.; Packham, G.; Ganesan, A. The First Biologically Active Synthetic Analogues of FK228, the Depsipeptide Histone Deacetylase Inhibitor. *J. Med. Chem.* **2007**, *50*, 5720–5726.

(34) Fernandez, S. M.; Lewis, M. C.; Pechenino, A. S.; Harburger, L. L.; Orr, P. T.; Gresack, J. E.; Schafe, G. E.; Frick, K. M. Estradiol-Induced Enhancement of Object Memory Consolidation Involves Hippocampal Extracellular Signal-Regulated Kinase Activation and Membrane-Bound Estrogen Receptors. *J. Neurosci.* **2008**, *28*, 8660–8667.

(35) Boulware, M. I.; Heisler, J. D.; Frick, K. M. The Memory-Enhancing Effects of Hippocampal Estrogen Receptor Activation Involve Metabotropic Glutamate Receptor Signaling. *J. Neurosci.* **2013**, *33*, 15184–15194.

(36) Tuscher, J. J.; Fortress, A. M.; Kim, J.; Frick, K. M. Regulation of Object Recognition and Object Placement by Ovarian Sex Steroid Hormones. *Behav. Brain Res.* **2015**, *285*, 140–157.

(37) De Simone, A.; Milelli, A. Histone Deacetylase Inhibitors as Multitarget Ligands: New Players in Alzheimer's Disease Drug Discovery? *ChemMedChem* **2019**, *14*, 1067–1073.

(38) Sharma, S.; Sarathlal, K. C.; Taliyan, R. Epigenetics in Neurodegenerative Diseases: The Role of Histone Deacetylases. *CNS Neurol. Disord.: Drug Targets* **2019**, *18*, 11–18.

(39) Yang, S.; Zhang, R.; Wang, G.; Zhang, Y. The Development Prospection of HDACi as a Potential Therapeutic Direction in Alzheimer's Disease. *Transl. Neurodegener.* **2017**, *6*, No. 19.

(40) Kazantsev, A. G.; Thompson, L. M. Therapeutic Application of Histone Deacetylase Inhibitors for Central Nervous System Disorders. *Nat. Rev. Drug Discovery* **2008**, *7*, 854–868.

(41) Kim, S. W.; Hooker, J. M.; Otto, N.; Win, K.; Muench, L.; Shea, C.; Carter, P.; King, P.; Reid, A. E.; Volkow, N. D.; Fowler, J. S. Whole-Body Pharmacokinetics of HDAC Inhibitor Drugs, Butyric Acid, Valproic Acid and 4-Phenylbutyric Acid Measured with Carbon-11 Labeled Analogs by PET. *Nucl. Med. Biol.* **2013**, *40*, 912–918.

- (42) Schroeder, F. A.; Wang, C.; Van de Bittner, G. C.; Neelamegam, R.; Takakura, W. R.; Karunakaran, A.; Wey, H. Y.; Reis, S. A.; Gale, J.; Zhang, Y. L.; Holson, E. B.; Haggarty, S. J.; Hooker, J. M. PET Imaging Demonstrates Histone Deacetylase Target Engagement and Clarifies Brain Penetration of Known and Novel Small Molecule Inhibitors in Rat. *ACS Chem. Neurosci.* **2014**, *5*, 1055–1062.
- (43) Ghosh, B.; Zhao, W.-N.; Reis, S. A.; Patnaik, D.; Fass, D. M.; Tsai, L.-H.; Mazitschek, R.; Haggarty, S. J. Dissecting Structure-Activity-Relationships of Crebinostat: Brain Penetrant HDACi for Neuroepigenetic Regulation. *Bioorg. Med. Chem. Lett.* **2016**, *26*, 1265–1271.
- (44) Luckhurst, C. A.; Breccia, P.; Stott, A. J.; Aziz, O.; Birch, H. L.; Bürlü, R. W.; Hughes, S. J.; Jarvis, R. E.; Lamers, M.; Leonard, P. M.; Matthews, K. L.; et al. Potent, Selective, and CNS-Penetrant Tetrasubstituted Cyclopropane Class IIa Histone Deacetylase (HDAC) Inhibitors. *ACS Med. Chem. Lett.* **2016**, *7*, 34–39.
- (45) Panicker, J.; Li, Z.; McMahon, C.; Sizer, C.; Steadman, K.; Piekarczyk, R.; Bates, S. E.; Thiele, C. J. Romidepsin (FK228/Depsipeptide) Controls Growth and Induces Apoptosis in Neuroblastoma Tumor Cells. *Cell Cycle* **2010**, *9*, 1830–1838.
- (46) Subramanian, S.; Bates, S. E.; Wright, J. J.; Espinoza-Delgado, I.; Piekarczyk, R. L. Clinical Toxicities of Histone Deacetylase Inhibitors. *Pharmaceuticals* **2010**, *3*, 2751–2767.
- (47) Wang, T.; Jia, Y.; Zhang, X.; Sun, Q.; Li, Y.-C.; Zhang, J.; Zhao, C.; Wang, X.; Wang, L. Treating Colon Cancer Cells with FK228 Reveals a Link between Histone Lysine Acetylation and Extensive Changes in the Cellular Proteome. *Sci. Rep.* **2016**, *5*, No. 18443.
- (48) Marchion, D. C.; Bicaku, E.; Daud, A. I.; Sullivan, D. M.; Munster, P. N. *In Vivo* Synergy between Topoisomerase II and Histone Deacetylase Inhibitors: Predictive Correlates. *Mol. Cancer Ther.* **2005**, *4*, 1993–2000.
- (49) Kumar, A.; Yegla, B.; Foster, T. Redox Signaling in Neurotransmission and Cognition During Aging. *Antioxid. Redox Signaling* **2018**, *28*, 1724–1745.
- (50) Hitchcock, S. A. Blood-brain barrier permeability considerations for CNS-targeted compound library design. *Curr. Opin. Chem. Biol.* **2008**, *12*, 318–323.
- (51) Tuscher, J. J.; Taxier, L. R.; Fortress, A. M.; Frick, K. M. Chemogenetic Inactivation of the Dorsal Hippocampus and Medial Prefrontal Cortex, Individually and Concurrently, Impairs Object Recognition and Spatial Memory Consolidation in Female Mice. *Neurobiol. Learn. Mem.* **2018**, *156*, 103–116.
- (52) Dickerson, B. C.; Eichenbaum, H. The Episodic Memory System: Neurocircuitry and Disorders. *Neuropsychopharmacology* **2010**, *35*, 86–104.
- (53) Gallagher, M.; Koh, M. T. Episodic Memory on the Path to Alzheimer's Disease. *Curr. Opin. Neurobiol.* **2011**, *21*, 929–934.
- (54) Alberini, C. M. Transcription Factors in Long-Term Memory and Synaptic Plasticity. *Physiol. Rev.* **2009**, *89*, 121–145.
- (55) Squire, L. R.; Genzel, L.; Wixted, J. T.; Morris, R. G. Memory Consolidation. *Cold Spring Harbor Perspect. Biol.* **2015**, *7*, No. a021766.
- (56) Roozendaal, B.; Hernandez, A.; Cabrera, S. M.; Hagewoud, R.; Malvaez, M.; Stefanko, D. P.; Haettig, J.; Wood, M. A. Membrane-Associated Glucocorticoid Activity Is Necessary for Modulation of Long-Term Memory via Chromatin Modification. *J. Neurosci.* **2010**, *30*, 5037–5046.
- (57) Frye, C. A.; Duffy, C. K.; Walf, A. A. Estrogens and Progestins Enhance Spatial Learning of Intact and Ovariectomized Rats in the Object Placement Task. *Neurobiol. Learn. Mem.* **2007**, *88*, 208–216.
- (58) Govindarajan, N.; Rao, P.; Burkhardt, S.; Sananbenesi, F.; Schlüter, O. M.; Bradke, F.; Lu, J.; Fischer, A. Reducing HDAC6 Ameliorates Deficits in a Mouse Model for Alzheimer's disease. *EMBO Mol. Med.* **2013**, *5*, 52–63.
- (59) Reolon, G. K.; Maurmann, N.; Werenicz, A.; Garcia, V. A.; Schröder, N.; Wood, M. A.; Roesler, R. Posttraining Systemic Administration of the Histone Deacetylase Inhibitor Sodium Butyrate Ameliorates Aging-Related Memory Decline in Rats. *Behav. Brain Res.* **2011**, *221*, 329–332.
- (60) Broadbent, N. J.; Squire, L. R.; Clark, R. E. Spatial Memory, Recognition Memory, and the Hippocampus. *Proc. Natl. Acad. Sci. U.S.A.* **2004**, *101*, 14515–14520.
- (61) Hammond, R. S.; Tull, L. E.; Stackman, R. W. On the Delay-Dependent Involvement of the Hippocampus in Object Recognition Memory. *Neurobiol. Learn. Mem.* **2004**, *82*, 26–34.
- (62) Wilson, D. I. G.; Langston, R. F.; Schlesiger, M. I.; Wagner, M.; Watanabe, S.; Ainge, J. A. Lateral Entorhinal Cortex Is Critical for Novel Object-Context Recognition. *Hippocampus* **2013**, *23*, 352–366.
- (63) Zhang, B.; Liu, J.; Gao, D.; Yu, X.; Wang, J.; Lei, X. A Fluorine Scan on the Zn<sup>2+</sup>-Binding Thiolate Side Chain of HDAC Inhibitor Lpargazole: Synthesis, Biological Evaluation, and Molecular Modeling. *Eur. J. Med. Chem.* **2019**, *182*, No. 111672.
- (64) Yamada, T.; Miki, S.; Ul'Husna, A.; Michikawa, A.; Nakatani, K. Synthesis of Naphthyridine Carbamate Dimer (NCD) Derivatives Modified with Alkanethiol and Binding Properties of G-G Mismatch DNA. *Org. Lett.* **2017**, *19*, 4163–4166.
- (65) Doi, T.; Otaka, H.; Umeda, K.; Yoshida, M. Study for Diastereoselective Aldol Reaction in Flow: Synthesis of (E)-(S)-3-Hydroxy-7-Tritylthio-4-Heptenoic Acid, a Key Component of Cyclo-depsipeptide HDAC Inhibitors. *Tetrahedron* **2015**, *71*, 6463–6470.
- (66) Narita, K.; Sayar, N.; Saijo, K.; Ishioka, C.; Katoh, T. A Concise Approach for Producing Optically Pure Carboxylic Acid Segments for the Synthesis of Bicyclic Depsipeptide Histone Deacetylase Inhibitors. *Synthesis* **2019**, *51*, 1408–1418.
- (67) Tuscher, J. J.; Szinte, J. S.; Starrett, J. R.; Krentzel, A. A.; Fortress, A. M.; Remage-Healey, L.; Frick, K. M. Inhibition of Local Estrogen Synthesis in the Hippocampus Impairs Hippocampal Memory Consolidation in Ovariectomized Female Mice. *Horm. Behav.* **2016**, *83*, 60–67.
- (68) Koss, W. A.; Haertel, J. M.; Philippi, S. M.; Frick, K. M. Sex Differences in the Rapid Cell Signaling Mechanisms Underlying the Memory-Enhancing Effects of 17 $\beta$ -Estradiol. *eNeuro* **2018**, *5*, No. ENEURO.0267-18.2018.
- (69) Frick, K. M.; Gresack, J. E. Sex Differences in the Behavioral Response to Spatial and Object Novelty in Adult C57BL/6 Mice. *Behav. Neurosci.* **2003**, *117*, 1283–1291.
- (70) Fortress, A. M.; Fan, L.; Orr, P. T.; Zhao, Z.; Frick, K. M. Estradiol-Induced Object Recognition Memory Consolidation Is Dependent on Activation of MTOR Signaling in the Dorsal Hippocampus. *Learn. Mem.* **2013**, *20*, 147–155.
- (71) Taxier, L. R.; Philippi, S. M.; Fortress, A. M.; Frick, K. M. Dickkopf-1 Blocks 17 $\beta$ -Estradiol-Enhanced Object Memory Consolidation in Ovariectomized Female Mice. *Horm. Behav.* **2019**, *114*, No. 104545.

## NOTE ADDED AFTER ASAP PUBLICATION

Originally published ASAP on February 8, 2022; Scheme 1 and 2 reagents and conditions updated February 9, 2022.